Spectroscopic characterization, DFT calculations, in vitro pharmacological potentials, and molecular docking studies of N, N, O-Schiff base and its trivalent metal complexes

Ikechukwu P. Ejidike
University of South Africa

Amani Direm
Université Abbes Laghrour Khenchela

Cemal Parlak
Ege Üniversitesi

Adebayo A. Adeniyi
University of the Free State

Mohammad Azam
College of Sciences

Authors

Ikechukwu P. Ejidike, Amani Direm, Cemal Parlak, Adebayo A. Adeniyi, Mohammad Azam, Athar Ata, Michael O. Eze, Joshua W. Hollett, and Hadley S. Clayton
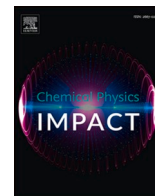
Full Length Article

Spectroscopic characterization, DFT calculations, *in vitro* pharmacological potentials, and molecular docking studies of *N, N, O*-Schiff base and its trivalent metal complexes

Ikechukwu P. Ejidike [a,b,c,*], Amani Direm [d,e], Cemal Parlak [f], Adebayo A. Adeniyi [g,h], Mohammad Azam [i], Athar Ata [b,j,**], Michael O. Eze [b], Joshua W. Hollett [b], Hadley S. Clayton [a]

[a] *Department of Chemistry, College of Science, Engineering and Technology, University of South Africa, Florida 1710, South Africa*
[b] *Department of Chemistry, Faculty of Science, The University of Winnipeg, Winnipeg, MB R3B 2E9, Canada*
[c] *Department of Chemical Sciences, Faculty of Natural, Applied and Health Sciences, Anchor University, Lagos 100278, Nigeria*
[d] *Laboratory of Structures, Properties and Interatomic Interactions LASPI2A, Faculty of Sciences and Technology, Abbes Laghrour University, Khenchela 40.000, Algeria*
[e] *Department of Matter Sciences, Faculty of Sciences and Technology, Abbes Laghrour University, Khenchela 40.000, Algeria*
[f] *Department of Physics, Faculty of Science, Ege University, Izmir 35040, Turkey*
[g] *Department of Chemistry, University of the Free State, PO Box 339, Bloemfontein 9300, South Africa*
[h] *Department of Industrial Chemistry, Faculty of Sciences, Federal University, Oye-Ekiti 371104, Nigeria*
[i] *Department of Chemistry, College of Science, King Saud University, Riyadh 11451, Saudi Arabia*
[j] *Department of Chemistry, College of Sciences and Arts, Michigan Technological University, Houghton, MI 49931, USA*

ABSTRACT

In this study, trivalent metal complexes of the category: $[M(L)(H_2O)_nCl_y]$ obtained from the interaction of metal^{3+} ion salts with organic *N, N, O*-Schiff base (**HL**) (where: **HL** = 4-{(*Z*)-((2-{(*E*)-((2-hydroxyphenyl)methylidene)amino}ethyl)imino)methyl}-2-methoxyphenol; n, *y* = 1 or 2 and *M* = Ti(III), Fe(III), Ru(III), Cr(III) and Al(III)) were synthesized and characterized *viz* molar conductance, FT-IR, and UV–Vis spectroscopies, elemental analyses, thermal analyses (TGA and DTA), and UV–Vis spectroscopy, theoretical calculations. A distorted octahedral structure around the metal ions was proposed based on the obtained experimental and calculated data. Thermal examination of the complexes signposts the step-by-step disintegration to give the final decomposition product as metal oxides. Moreover, DFT calculations were executed utilizing the B3LYP/LANL2DZ theory level, which revealed that the synthesized metal (III) complexes were more stable than the free ligand (**HL**). The value of ΔE for **HL** is 4.60 eV while the related values for the complexes of Cr(III) (**C1**), Ru(III) (**C2**), Fe (III) (**C3**), Al(III) (**C4**), and Ti(III) (**C5**) are respectively 2.59, 3.68, 3.15, 1.64, and 2.75 eV. Scavenging abilities of DPPH and ABTS radicals by the test compounds revealed promising antioxidant behavior. It was observed that the compounds are proficient DPPH radical scavengers in a dose-dependent configuration. Ru(III); IC$_{50}$ = 1.69 ± 2.68 μM for DPPH and Ti(III); IC$_{50}$ = 8.70 ± 2.78 μM for ABTS performed best. Similarly, the complexes demonstrated higher antimicrobial activities compared to **HL** against the designated strains, while ciprofloxacin acted as a standard antibiotic. Furthermore, the ligand and its most effective complexes **C2** and **C5** were docked against the targets *S. aureus* DNA gyrase (**2XCT**), *S. pneumoniae* DNA gyrase (**5BOD**), and E. *coli* DNA gyrase (**5L3J**). The binding sites were evaluated and the docking results showed that the studied molecules bind to the targets through classical O—H…O and/or N—H…O hydrogen bonds, as well as *via* hydrophobic contacts.

1. Introduction

Schiff bases are a significant set of organic compounds specially studied owing to their various applications [1]. Tridentate donor ligands formed by heterocyclic Schiff bases have displayed some metal complexes stabilization character, having the coordination to occur *via* the

nitrogen and oxygen-donor atoms [2]. They are categorized as organic ligands resulting from amines (primary or secondary) and equivalent ketones or aldehydes condensation reactions [3,4]. The derivatives of Schiff base ligands display a variety of biological activities owing to the azomethine linkage, responsible for several antibacterial, clinical, anti-fungal, herbicidal, anticancer, and analytical activities [1–4]. Bio-active complexes bearing Schiff base originating from vinyl aniline, aliphatic or aromatic diamines, and heterocyclic aldehydes like 4-hydroxy-3-methoxybenzaldehyde, 3,4-dimethoxybenzaldehyde, 2-hydroxy-1-napthaldehyde have received recognition owing to their favourable antimicrobial activities. As such, chelation enhances the biological capabilities of synthesized metal compounds [2,6–9].

Metal-organic compounds play a critical role in many biological systems, and it has been well-known that various organic compounds utilized in medicine are triggered by metal ion metabolism [2–4]. Oxygen and nitrogen donor Schiff bases transition metal complexes are of interest, because of their ability to adopt an uncommon configuration. These complexes have potential applications in clinical, analytical, and industrial processes, and play a key role in biological systems [4,5]. Schiff base complexes of trivalent metallic centers, such as Cr(III), Eu (III), Fe(III), In(III), Ir(III), Ru(III), Co(III), Sm(III), Ti(III), Ga(III), Os (III), Mn(III), and Al(III) have enticed considerable attention and demonstrated excellent biological properties [5,6,8,10–18]. Other metal-organic compounds [18,19] such as flower-like organic-inorganic materials synthesized by the simultaneous coordination-driven assembly of heterocyclic molecules and porous materials-magnesium film coated with the self-assembled (8-hydroxyquinoline) exhibited superior corrosion protection bare magnesium [18]; while hybrid organic-inorganic (HOI) materials consisting of micro composites supported on metals, ceramics, or polymers have displayed better catalytic, electrochemical, or biological performance [20,21]. The catalytic properties of tridentate Schiff base copper complex have been reported for the cycloaddition promotion of a Cu(II) bound SCN^- ion to 2-pyridyl-N-(2'-methylthiophenyl) methyleneimine that stoichiometrically forms a mesoionic imidazo[1,5-a]pyridine in acetonitrile solution [22].

Anti-oxidants are considered crucial nutraceuticals because of their health assistance and are extensively used in the food industry [4,9]. Physiological and biochemical procedures are the trail for the cohort of reactive oxygen species (ROS) within active body cells [1]. Metal-Schiff base complexes derived anti-oxidants are currently receiving attention for their competence to defend cells from injury as a result of free radicals [4,9,23,24]. Series of metal(II)-Schiff base complexes with ligands gained from 4-aminoantipyrine with furfural and amino acids (glycine, alanine, and valine) condensation were reported [8]. The antioxidant activity of Zn(II) and Ni(II) complexes exhibited good hydroxyl radical scavenging capability [8].

The free-radical scavenging ability of Co(II), Ni(II), and Cu(II) chlorides complexes with f-(Z)−2-(pyrrolidin-2-ylidene)hydrazinecarbothioamide were appraised for their ability to interact with the steady free radical- 1,1-diphenyl-2-picrylhydrazyl (DPPH); the test agents revealed potential anti-oxidant activities [23]. Anti-oxidant studies of four mononuclear Ru(III) complexes of 2′,4′-dihydroxyacetophenone derived Schiff bases demonstrated electron or hydrogen atom donors potential, and subsequently put an end to the chain reactions in a dose-manner-method [15]. In another study, the radical scavenging accomplishments of Ni^{2+}, Cu^{2+}, and VO^{2+} complexes gotten with 4,4′-bis-({2-[(2-hydroxy-phenylamino)-methyl]-benzylidene}-amino)-biphenyl-3,3′-diol Schiff base has shown that the free ligand radical activity was considerably improved upon complex formation with metal ions [25]. Schiff base derived from dopamine: (4-{2-[(2-hydroxy-benzylidene)-amino]-ethyl}-benzene-1,2-diol) and its transition metal- Pd(II), Pt(IV), and Ni(II) complexes exhibited antioxidant potentials using the DPPH radical scavenging method [26].

Molecular docking studies and biological activity of inner metal- La (III), Yb(III), and Er(III) complexes of tetradentate (ONNO) Schiff base: 2,2′-((1E,1′E)-(1,3-phenylenebis(azanylylidene))bis(methanylylidene))

diphenol have been reported to possess better antimicrobial activities against different organisms compared to the free ligand (Gram (+ve) bacteria- *Bacillus subtilis* and *Staphylococcus aureus;* Gram (-ve) bacteria- *Escherichia coli, Salmonella* sp., and *Pseudomonas aeruginosa;* as well as fungi- *Aspergillus fumigatus* and *Candida albicans*). The compounds showed effective and possible binding modes with different active sites of PDB code: 2hq6 (colon cancer) and PDB code: 1 × 2j (lung cancer) receptors [27]. Crystal Structure, Hirschfeld surface, spectroscopic analysis, and molecular docking of hexahydroquinoline derivative (HQ) and 2-amino thiophene derivative have stressed adequate charge transfer/ electron transport within the molecules owing to their HOMO and LUMO energies. Seven protein receptors were utilized for the molecular docking, while best ligand-protein interactions drug-likeness analysis [28,29].

In another study by Zayed and co-workers, molecular docking of bis-Schiff base ligand (H₂L): [4,4′-((((ethane-1,2-diylbis(oxy))bis(2,1-phenylene))bis(methanylylidene))bis(azanylylidene))diphenol]ethane and its Cu(II), Mn(II), Zn(II), Ni(II), Co(II), Fe(III), and Cd(II) complexes was achieved using AutoDock tools to explain the experimental behavior of the Schiff base ligand towards proteins of *E. coli* (3t88), *Bacillus subtilis* (5h67), *Staphylococcus aureus* (3ty7), and *Proteus vulgaris* (5i39) microorganisms through theoretical calculations, while DFT/B3LYP method was utilized for the energy gaps and other important theoretical parameters, and *in vitro* antibacterial studies against several organisms, both Gram negative (*P. vulgaris* and *E. coli*) and Gram positive (*S. pyogones* and *B. subtilis*) [30].

In an effort towards developing metallic-based chemotherapeutic agents, we convey the reaction and characterization of the Schiff base ligand: 4-{(Z)-[2-{(E)-[(2-hydroxyphenyl)methylidene]amino}ethyl) imino]methyl}−2-methoxyphenol (**HL**) obtained by the condensation of 2-hydroxybenzaldehyde and *o*-vanillin with aliphatic diamine and its corresponding trivalent metal: Cr(III), Ru(III), Fe(III), Ti(III) and Al(III) complexes. The synthesized ligand **HL** and its metal(III) coordination complexes were characterized by techniques including elemental analysis, Fourier transform infrared (FT-IR), molar conductance, ultraviolet-visible (UV–Vis), melting point, thermogravimetric (TG), and differential thermogravimetric (DTG) analyses studies. The molecular structures of **HL** and its complexes **C1**-**C5** were optimized and their frontier molecular orbitals were energies estimated by density functional theory (DFT) *via* the B3LYP/LANL2DZ method. The *in vitro* free radical scavenging potential and antimicrobial screening of the asymmetrical tridentate Schiff base ligand **HL** and its metal chelates against *E. coli, α-H. streptococcus, S. aureus, A. candideus, P. cephalosporin,* and *A. niger* were evaluated. Furthermore, the most effective complexes **C2** and **C5** together with the free ligand **HL** were docked, based on the *in vitro* results, in the binding pockets of *Staphylococcus aureus* topoisomerase II DNA gyrase A (PDB ID: **2XCT**), *Streptococcus pneumoniae* topoisomerase II DNA gyrase B (PDB ID: **5BOD**) and E. *coli* topoisomerase II DNA gyrase B (PDB ID: **5L3J**), as an attempt to showcase the interactions binding the studied molecules to the tested strains.

2. Materials and methods

2.1. Materials

Chemicals and solvents were of annular grade and were used deprived of advanced purification before syntheses. 2-hydroxybenzaldehyde, ethylenediamine, $CrCl_3 \bullet 6H_2O$, $FeCl_3 \bullet 6H_2O$, $RuCl_3 \bullet xH_2O$, *o*-vanillin were received from Merck (Johannesburg, South Africa), while $AlCl_3 \bullet xH_2O$, $TiCl_3$, Gallic acid, ascorbic acid were received from Sigma-Aldrich (Johannesburg, South Africa). 2,2′-azinobis-3-ethyl-benzothiazoline-6-sulfonic acid- ABTS, rutin hydrate, and 1,1-Diphenyl-2-picrylhydrazyl- DPPH were procured from Sigma-Aldrich Chemical Co. (USA). Perkin Elmer-Spectrum 2000 FT-IR spectrometer within the range 4000–400 cm^{-1} was used for IR spectra generation. Freshly prepared 10^{-3} M DMF solutions of the complexes at 298 K via a PC 7000
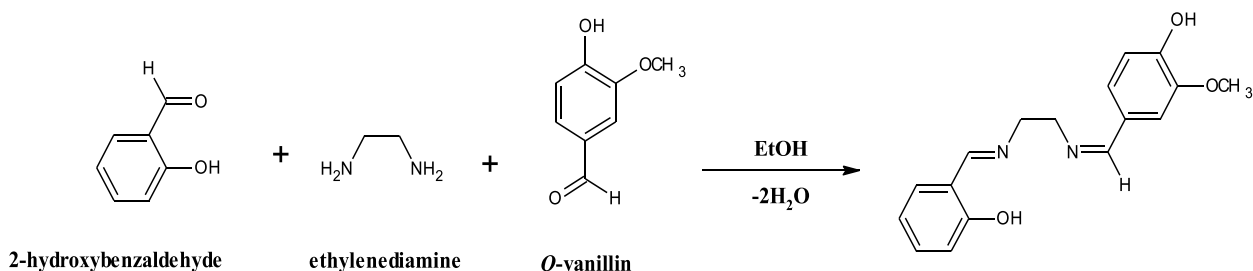
Scheme 1. Synthesis of the Schiff base ligand (HL).
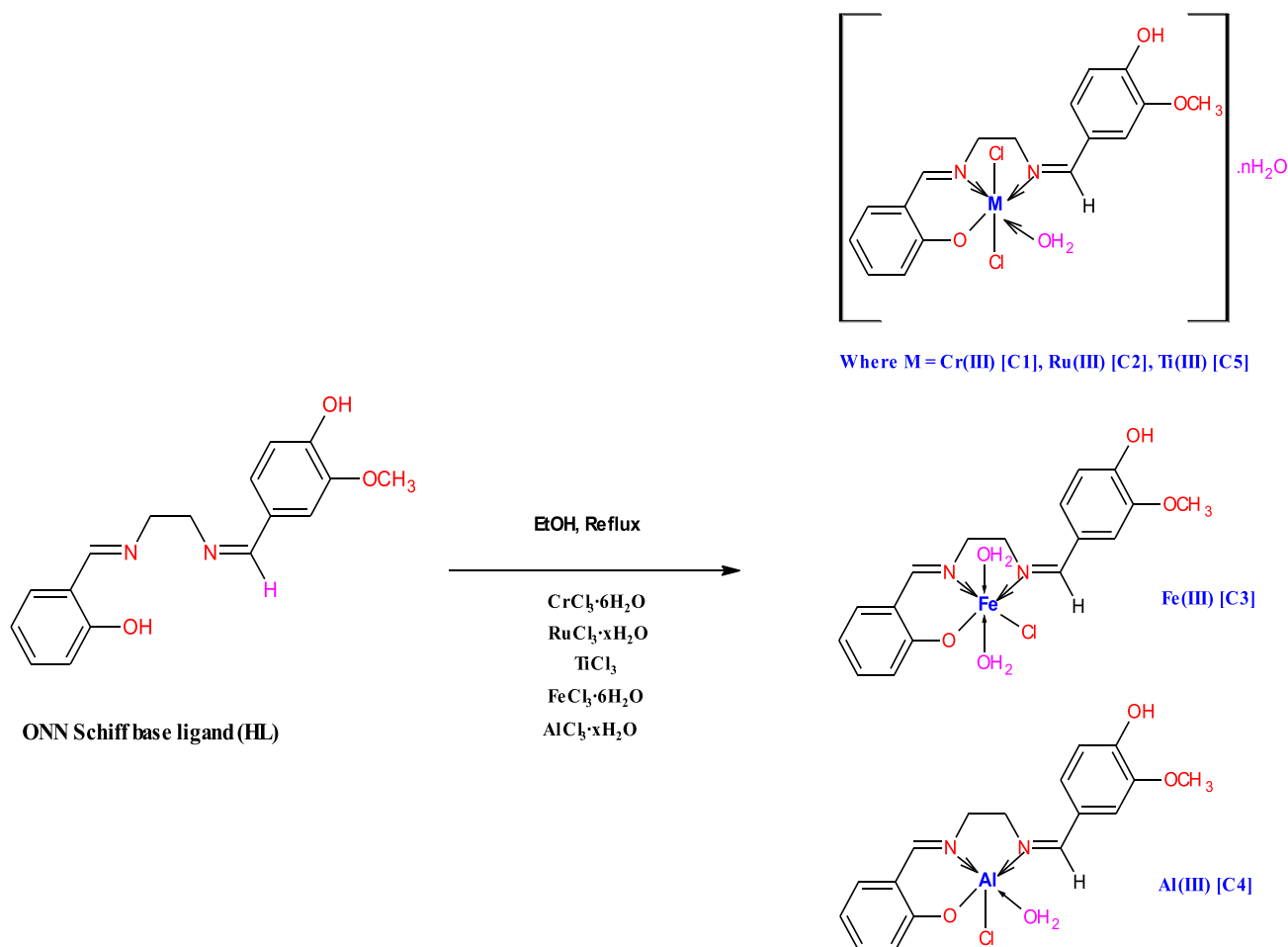
Scheme 2. Synthetic pathway and proposed structures of the Metal(III) complexes of ONN Schiff base ligand (HL).

conductivity cell (EUTECH, Tuas, Singapore) were evaluated for conductivity measurements. SMP 10 Melting Point Apparatus (Stuart, Chelmsford, UK) was utilized for the melting points. The studies of C, H, and N were investigated on a Perkin Elmer-Elemental analyzer (Waltham, MA). Thermal disintegration studies of the as-synthesized complexes were recorded on Perkin Elmer-Thermogravimetric analyzer: TGA 4000 System (Waltham, MA, USA). UV–Vis spectrometer-model T80+ (PG Instruments Ltd., Leicestershire, UK) was utilized for the electronic spectra examination in the 200–800 nm range.

2.2. Synthesis of the ligand: 4-{(Z)-[(2-{(E)-[(2-hydroxyphenyl) methylidene]amino}ethyl) imino]methyl}−2-methoxyphenol (HL)

A typical technique as per previous reports [4,9] was tailed for the Schiff base synthesis (Scheme 1): A slow addition of 30 mL ethanolic solution of ethylenediamine (0.02 mol) to 50 mL ethanolic solution comprising 2-hydroxybenzaldehyde (0.02 mol), followed by the drop-wise addition of 40 mL o-vanillin (0.02 mol) in ethanolic solution. The coloured combination was stirred and refluxed for 4 h, and permitted to agitate at room temperature additionally for several minutes and the subsequent cool precipitate was sieved, severally washed with ethanol, and recrystallized from warm ethanolic solution. Yield: 4.58 g (76.70 %); Brownish-yellow solid; F. Wt: 298.34 g; m. pt., 144–146 °C; Anal. Calcd. for $C_{17}H_{18}N_2O_3$ (%): C: 68.44, H: 6.08, N: 9.39; Found (%): C: 68.81, H: 5.89, N: 9.61; IR ν_{max}/cm^{-1}: 748 (C–H) in plane, 1160 (C–O–C), 1286 (C–O), 1596 (C=C), 1631 (C=N), 2868 (C–H) aliph., 2960 (C–H)arom., 3448 (Ar–OH); UV–Vis (DMF): λ_{max}/nm (cm^{-1}): 295 (33 898), 320 (31 250), 410 (24 390).

2.3. Overall procedure for the complexes (C1-C5) synthesis

Complexes **C2**-**C5** were obtained by the addition of 0.002 mol of CrCl$_3$•6H$_2$O, FeCl$_3$•6H$_2$O, RuCl$_3$•xH$_2$O, TiCl$_3$, or AlCl$_3$•xH$_2$O liquefied in 20 mL absolute ethanol to a pre-warmed ethanolic solution of the ligand (0.002 mol, 0.5967 g, 50 mL). A color change was observed within some minutes. Refluxing of the subsequent mixtures for 5-6 h (Scheme 2), generated solids that were sieved off from the reaction mixture after cooling, washed with cold ethanol, followed by diethyl ether, and dehydrated over anhydrous calcium chloride [1,3].

2.3.1. Synthesis of [C$_6$H$_4$O:CH:N(C$_2$H$_4$)N:CH:C$_6$H$_3$OHOCH$_3$CrCl$_2$(H$_2$O)] (C1)

[Cr(L)(H$_2$O)Cl$_2$]. Dark-green Solid; Yield: 463.8 mg (52.92 %); F. Wt: 438.25 g; Anal. Calcd. for C$_{17}$H$_{19}$Cl$_2$N$_2$O$_4$Cr (%): C: 46.59, H: 4.37, N: 6.39; Found (%): C: 47.02, H: 4.61, N: 6.74; IR ν_{max}/cm^{-1}: 3345 (O-H), 2904 (C–H)arom., 2802 (C–H)aliph., 1601 (C=N), 1584 (C=C), 1241 (C-O), 1125 (C–O–C), 733 (C–H) in plane, 533 (Cr-N), 470 (Cr-O); UV–Vis (DMF): λ$_{max}$/nm (cm^{-1}): 295 (33 898), 315 (31 746), 330 (30 303), 385 (25 974), 410 (24 390), 440 (22 727); Decomp. Temp.: 177–178 °C; Λµ: 33.60 µScm^{-1}.

2.3.2. Synthesis of [C$_6$H$_4$O:CH:N(C$_2$H$_4$)N:CH: C$_6$H$_3$OHOCH$_3$RuCl$_2$(H$_2$O)] (C2)

[Ru(L)(H$_2$O)Cl$_2$]·H$_2$O. Darkish-brown Solid; Yield: 781.0 mg (77.27 %); F. Wt: 505.34 g; Anal. Calcd. for C$_{17}$H$_{21}$Cl$_2$N$_2$O$_5$Ru (%): C: 40.41, H: 4.19, N: 5.54; Found (%): C: 40.86, H: 3.83, N: 5.81; IR ν_{max}/cm^{-1}: 3420 (O—H), 3061 (C–H)arom., 2974 (C–H)aliph., 1647 (C=N), 1598 (C=C), 1280 (C—O), 1153 (C–O–C), 763 (C–H) in plane, 594 (Ru-N), 460 (Ru-O); UV–Vis (DMF): λ$_{max}$/nm (cm^{-1}): 295 (33 898), 325 (30 769), 395

N: 6.45; Found (%): C: 46.72, H: 4.87, N: 6.96; IR ν_{max}/cm^{-1}: 3399 (O-H), 2902 (C–H)arom., 2803 (C–H)aliph., 1602 (C=N), 1564 (C=C), 1250 (C-O), 1149 (C–O–C), 760 (C–H) in plane, 531 (Ti-N), 475 (Ti-O); UV–Vis (DMF): λ$_{max}$/nm (cm^{-1}): 295 (33 898), 310 (32 258), 315 (31 746), 360 (27 778), 405 (24 691); Decomp. Temp.: 209–211 °C; Λµ: 31.10 µScm^{-1}.

2.4. DFT calculations

The theoretical calculations including the representations of the frontier orbitals HOMO and LUMO were performed using Gaussian 09 W and Gauss View 6.0 software for the synthesized ligand (**HL**) and its corresponding Ru(III), Cr(III), Fe(III), Ti(III), and Al(III) complexes (**C1-C5**) [31,32]. The molecular morphologies and chemical structures of all the synthesized complexes were optimized using the B3LYP/LANL2DZ scheme in the gas phase.

2.5. Antioxidant assay

2.5.1. DPPH: 2,2-Diphenyl-1-picrylhydrazyl radical scavenging potential

DPPH (2,2-Diphenyl-1-picryl-hydrazyl) radical scavenging assessment is a quick system for the selection of radical scavenging performance. The as-synthesized (**C1-C5**) compounds (100, 200, 300, 400, or 500 µg/mL) using a previous method were investigated by quantifying the reduction in the radical solution absorbance at 517 nm [4,17,25]. Gallic acid and vitamin C served as standard samples. All test samples were completed in triplicate to achieve the mean ± *S*.D. This assessment was premeditated using the equation below:

$$\%DPPH \ radical \ scavenging \ ability = \frac{Absorbance \ of \ control - Absorbance \ of \ sample}{Absorbance \ of \ control} X100 \tag{1}$$

(25 316), 450 (22 222), 520 (19 231), 660 (15 152); Decomp. Temp.: 191–193 °C; Λµ: 30.40 µScm^{-1}.

2.3.3. Synthesis of [C$_6$H$_4$O:CH:N(C$_2$H$_4$)N:CH:C$_6$H$_3$OHOCH$_3$FeCl(H$_2$O)$_2$] (C3)

[Fe(L)(H$_2$O)$_2$Cl]. Dark purple Solid; Yield: 533.8 mg (62.85 %); F. Wt: 424.66 g; Anal. Calcd. for C$_{17}$H$_{21}$ClN$_2$O$_5$Fe (%): C: 48.08, H: 4.98, N: 6.60; Found (%): C: 48.47, H: 4.69, N: 6.93; IR ν_{max}/cm^{-1}: 3393 (O—H), 2903 (C–H)arom., 2801 (C–H)aliph., 1628 (C = N), 1598 (C = C), 1246 (C—O), 1126 (C–O–C), 757 (C–H) in plane, 538 (Fe-N), 431 (Fe-O); UV–Vis (DMF): λ$_{max}$/nm (cm^{-1}): 305 (32 787), 325 (30 769), 390 (25 641), 420 (23 809), 485 (20 619), 520 (19 231); Decomp. Temp.: 235–236 °C; Λµ: 33.90 µScm^{-1}.

2.3.4. Synthesis of [C$_6$H$_4$O:CH:N(C$_2$H$_4$)N:CH:C$_6$H$_3$OHOCH$_3$AlCl(H$_2$O)] (C4)

[Al(L)(H$_2$O)Cl]. Cream-whitish Solid; Yield: 448.2 mg (59.32 %); F. Wt: 377.78 g; Anal. Calcd. for C$_{17}$H$_{19}$ClN$_2$O$_4$Al (%): C: 54.05, H: 5.07, N: 7.42; Found (%): C: 54.49, H: 5.52, N: 7.84; IR ν_{max}/cm^{-1}: 3365 (O-H), 2906 (C–H)arom., 2804 (C–H)aliph., 1600 (C=N), 1585 (C=C), 1267 (C-O), 1155 (C–O–C), 734 (C–H) in plane, 539 (Al-N), 474 (Al-O); UV–Vis (DMF): λ$_{max}$/nm (cm^{-1}): 295 (33 898), 310 (32 258), 325 (30 769), 420 (23 809); Decomp. Temp.: 223–224 °C; Λµ: 34.40 µScm^{-1}.

2.3.5. Synthesis of [C$_6$H$_4$O:CH:N(C$_2$H$_4$)N:CH:C$_6$H$_3$OHOCH$_3$TiCl$_2$(H$_2$O)] (C5)

[Ti(L)(H$_2$O)Cl$_2$]. Yellowish-orange Solid; Yield: 521.5 mg (60.07 %); F. Wt: 434.12 g; Anal. Calcd. for C$_{17}$H$_{19}$Cl$_2$N$_2$O$_4$Ti (%): C: 47.03, H: 4.41,

2.5.2. ABTS-2,2'-Azino-bis(3-ethylbenzothiazoline-6-sulfonic acid) radical scavenging assay

ABTS scavenging ability of the Ti(III), Ru(III), Cr(III), Fe(III), and Al (III)-tridentate Schiff base complexes (**C1-C5**) was screened using a previously described method with a 0.706 ± 0.001 units absorbance at 734 nm [1,4]. An equal volume of the tested samples (**C1-C5**) was mixed with ABTS$^+$ solution. The scavenging ability of the test agents alongside the standard drugs (Gallic acid and rutin hydrate) was assessed. The analysis was carried out in triplicate and the percentage inhibition was calculated.

2.6. Antimicrobial activity

A previously conveyed technique was followed for the antimicrobial screening [33,34]. The synthesized ligand (**HL**) and its corresponding complexes (**C1-C5**) were screened *vis-a-vis* the disk diffusion plate method. The selected bacterial strains: *E. coli, α-hemolytic streptococcus*, and *Staphylococcus aureus* were used for this investigation. The compounds were also screened against fungi kinds, namely: *Aspergillus candideus, Penicillium cephalosporin*, and *Aspergillus niger*. Pure cultures of bacteria were sub-cultured on sterile Nutrient Agar, while sterile Potato Dextrose Agar (PDA) was used for fungi species sub-culture. Sterile cotton swabs were used for each strain uniform swabbing onto individual plates. The compounds were dissolved in their suitable solvent at certain concentrations. Sterile paper discs containing the samples alongside the standard antibiotics: Ciprofloxacin and Fluconazole were placed on each plate. Incubation was allowed at 37 °C for 24 h for antibacterial assessment, and at 25 °C, for 24 h for antifungal activity.
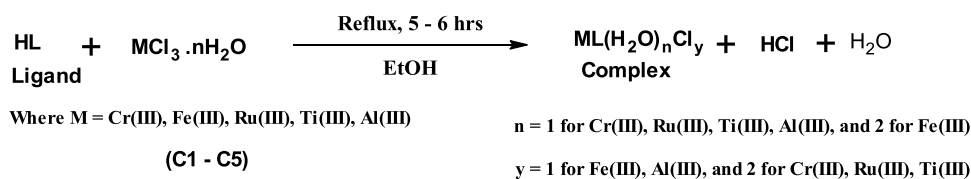
Zones of Inhibition (ZOI) were then determined.

2.7. Molecular docking

All the molecular docking designs were accomplished using Auto-Dock 4.2 software and AutoDock Tools ADT [35]. Based on the *in vitro* results and in an attempt to emphasize the interactions binding the studied molecules to the tested strains, we have docked **HL, C2** and **C5** against *Staphylococcus aureus* topoisomerase II DNA gyrase A, *Streptococcus pneumoniae* topoisomerase II DNA gyrase B and E. *coli* topoisomerase II DNA gyrase B, with the respective PDB IDs: **2XCT** [36], **5BOD** [37] and **5L3J** [38]. Type II DNA topoisomerase are essential enzyme found in both prokaryotes and eukaryotes [39]. Prokaryotic DNA gyrase topoisomerases have been shown to play a fundamental role in bacterial cell viability through their DNA replication commencement and negative supercoils introduction into the DNA during replication [40,41]. Therefore, such enzymes showed a big interest since they were thought to be attractive targets in designing new antibacterial drugs. The X-ray crystal structures of all the tested targets were acquired from the RCSB protein data bank [42], pickled by removing the co-crystallized inhibitors and their non-polar hydrogens merged in ADT [35]. Moreover, we have prepared the PDBQT format files by evaluating the rotatable bonds of the ligands and apportioning the *Gasteiger* and the *Kollman* charges to the correlated structures. The docking results were then visualized using Chimera software [43] and the Ligplot program [44], to analyze the interactions built up in the resulting target-ligand's pockets.

3. Results and discussion

3.1. Synthesis

The synthesis of the Schiff base (**HL**) and its metal(III) complexes can be exemplified by the equation below:

$$\text{HL} + \text{MCl}_3 \cdot n\text{H}_2\text{O} \xrightarrow[\text{EtOH}]{\text{Reflux, 5 - 6 hrs}} \text{ML(H}_2\text{O)}_n\text{Cl}_y + \text{HCl} + \text{H}_2\text{O}$$

HL Ligand + **MCl₃·nH₂O** → **ML(H₂O)ₙClᵧ** Complex + HCl + H₂O

Where M = Cr(III), Fe(III), Ru(III), Ti(III), Al(III)

(C1 - C5)

n = 1 for Cr(III), Ru(III), Ti(III), Al(III), and 2 for Fe(III)

y = 1 for Fe(III), Al(III), and 2 for Cr(III), Ru(III), Ti(III)

The synthesized Schiff base ligand (Fig. 1) and the proposed complexes (**C1-C5**) molecular structures are given in Scheme 2. The isolated complexes are of coloured powders, insoluble in H$_2$O and other common solvents, however, they are soluble in polar coordinating solvents like Dimethylsulfoxide (DMSO) and Dimethylformamide (DMF). The physico-analytical information and the molar conductance data of the ligand and its metal complexes as described represent a good treaty with the proposed formulation.

3.2. Molar conductivity measurements

The conductivity values (Λ_μ) of (**C1–C5**) complexes are recorded in 10^{-3} DMF solution. The results showed the molar conductance of the metal complexes solutions to be in the range of 30.40–34.40 μScm^{-1} indicating that the compounds are non-electrolytes at room temperature [2–5]. All the studied complexes exhibited low molar conductivity that could be attributed to the anionic coordination ring's low ionic mobility owning the bulky size [1–6,34,45].

3.3. Infrared spectral studies of the M(III) complexes

The Schiff base (**HL**) disclosed a broad band at 3448 cm^{-1}, which is attributable to the ν(O—H) vibration. This band disappearance in all the complexes (**C1-C5**) spectra is an indication that the chelation takes place *via* the enolic –OH group [1–3,5,15,24]. An appearance of broad bands in the 3345–3420 cm^{-1} section was detected in the complexes' spectra, indicating the existence of coordinated H$_2$O molecules [9,13–15]. The bands in the region of 815–860 cm^{-1} may also be apportioned to the out-of-plane bending and stretching vibrations of the coordinated water [13,15]. Also, the free ligand spectrum revealed a sharp strong group at 1631 cm^{-1} that could be ascribed to the ν(C=N) broadening of the azomethine cluster per previous reports [3–5,11–15]. In all the complexes, this ν(C=N) band moved to lower wavenumbers 1600–1647 cm^{-1} by about 3–31 cm^{-1}, suggesting the involvement of the azomethine nitrogen atom in the coordination ring with the metallic centers in the complexes (**C1–C5**) [1,7,10].

A medium band agreeing to phenolic ν(C-O) oxygen atom was detected at 1286 cm^{-1} in the free ligand spectrum. The lower shifting of the ν(C-O) stretching (1241–1280 cm^{-1}) as noticed in the metal(III) complexes spectra advocates that the phenolic OH group of the ligand (**HL**) is involved in coordination with metal ions after the deprotonation and formation of the C—O—M bond [4,6]. The aromatic sphere skeletal stretching (C=C) was constant in all compounds and not distorted upon complex formation as expected. Furthermore, the low-frequency skeletal bands pragmatic between 531 and 594 cm^{-1} are recognized to ν(M-N=C) and those inside the group of 431–475 cm^{-1} are apportioned to the ν(M—O) stretching [1,4,13–15,34]. The infrared spectra information established that the Schiff base (**HL**) exhibits tridentate binding mode *via* the two imino nitrogen groups and the phenolic oxygen atom.

The plots of the experimental and theoretical IR spectra are shown in Fig. S1 and their overlay is provided in the electronic supplementary information file (Fig. S2). The overlay of the experimental and theoretical IR spectra shows that many of the vibrations in the fingerprint area that define the metal-ligand bonds are significantly reproduced as evident in the alignment of the experimental and theoretical bands. The major variation in the experimental and theoretical exit beyond 3000 cm^{-1}, as only theoretical spectra of the ligand and complexes show significant bands around those areas that are absent in the experimental spectra, following the difference used to obtain each one.

3.4. Electronic absorption spectroscopy

The UV–Visible bands of the Schiff base (**HL**) and its trivalent metal (**C1-C5**) complexes were documented in DMF solution at 298 K within the range of 900–200 nm and presented in Fig. 2. The bands at 24 390, 31 250, and 33 898 cm^{-1} are accrediting to intraligand n-π^* and π-π^* transitions in the free ligand spectra [3–5,14–17,23–25]. The high spin Fe(III) complexes (**C3**) with d^5 configuration exhibit the ground state ^{6}A$_{1g}$ and the *d-d* transitions are spin-forbidden [5,11]. The electronic spectra of [Fe(L)(H$_2$O)$_2$Cl] complex exhibited groups at 19 231, 20 619, and 23 809 cm^{-1}. The first two bands are transferable to the ^{6}A$_{1g}$ → ^{4}T$_{2g}$(G) and ^{6}A$_{1g}$(G) → ^{4}T$_{1g}$(G) transitions characteristic of octahedral geometry around Fe(III) ions [5,11–13]. The third absorption band with low energy observed at 23 809 cm^{-1} is assigned to a charge-transfer
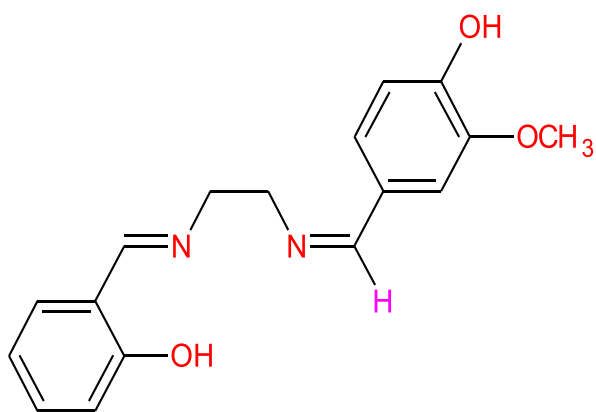
Fig. 1. Structure of 4-{(Z)-((2-{(E)-((2-hydroxyphenyl)methylidene)amino}ethyl)imino)methyl}−2-methoxyphenol (HL).

transition, LMCT, or MLCT [5,11,13]. Broad band with low-intensity at 24 691 cm^{-1} has been endorsed to $^2T_{2g} \rightarrow {}^2E_g$ transition for Ti (III)-complex. The band around 27 778 cm^{-1} could be attributed to a charge transfer L → M (LMCT) transition. The location and figure of the bands proposed an octahedral geometry distortion around the Ti(III) ion [10].

The electronic spectra of the $(Cr(L)(H_2O)Cl_2)$ complexes (**C1**) showed bands at around 25 974, 24 390, and 22 727 cm^{-1} that may be assigned to $^4A_{2g} \rightarrow {}^4T_{1g}(P)$, $^4A_{2g} \rightarrow {}^4T_{1g}(F)$, and $^4A_{2g} \rightarrow {}^4T_{2g}(F)$ transitions, respective1y. The locations of the band advocated an octahedral geometry for the Cr(III)-complex [5,10,12,13]. The Al(III) complex (**C4**) exhibited one band around 23 809 cm^{-1} which could be owed to the charge-transfer transitions, L → M (LMCT) [7,14]. The wide, strong, and poorly resolved groups between 385–480 nm could be allocated to LMCT [1,3,4]. The high-intensity band beneath 320 nm might be apportioned to an intraligand n–π*/π–π* transition [3]. d^5 electronic configuration of ruthenium(III) ion possesses moderately high oxidizing properties, and the ground state is $^2T_{2g}$. The foremost excited doublet

Fig. 2. Electronic absorption spectra of HL and its trivalent metal complexes.

levels of $^2A_{2g}$ and $^2T_{1g}$, arising from $t_{2g}^4 e_g^1$ configuration are in the mandate of increasing energy [15]. The Ru(III)-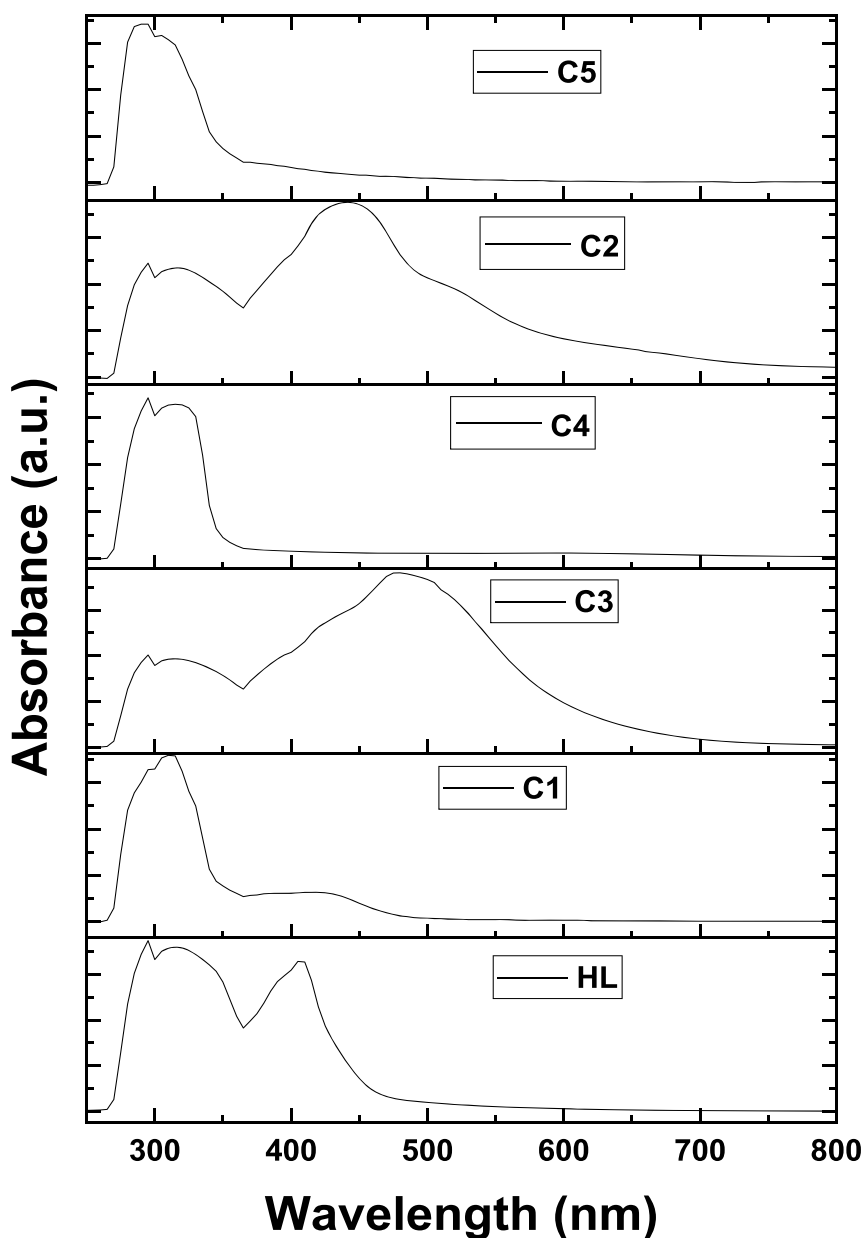Schiff base complex (**C2**) exhibits three electronic transition bands at 15 152, 19 231, and 22 222 cm^{-1} that have been assigned to $^2T_{2g} \rightarrow ^4T_{1g}$, $^2T_{2g} \rightarrow ^4T_{2g}$, and $^2T_{2g} \rightarrow ^2A_{1g}$ transitions, respective1y. The absorption pattern observed in the spectrum of the Ru(III) complex indicates an octahedral environment around the Ru^{3+} ion and agrees with the transition made for comparable octahedral ruthenium(III) complexes [15,16].

3.5. Thermal analysis

The thermal degradation of trivalent (**C1-C5**) complexes was deliberated using thermogravimetric procedures. TG/DTA of the as-synthesized Schiff base metal(III) compounds were scaled from 20 to 900 °C at a heating rate of 10 °C/ min under a nitrogen atmosphere (Fig. 3). TG outcomes designed as percentage weight loss against temperature afford an understanding of the nature, different molecules properties, and the obtained residues after thermal disintegration [2,11,13]. The complexes' decomposition occurred in different steps. The water molecules were present as lattice water and/or coordinated water. In the case of lattice water, lower temperature regions between 45 and 100 °C were required for its removal, whereas the loss of coordinated water requires temperatures of 120 °C or higher (Table 1). The TG/DTA curves revealed that the thermal decomposition of (**C1**), (**C2**), and (**C5**) occurred in one step, two steps, and four steps, respectively, whereas, for (**C3**) and (**C4**), the decomposition occurred in three steps. For the Ru(III) complex, the first decomposition step with a mass loss of 5.51 % (calcd. 5.82 %) and 17.64 % (calcd. 17.97 %) in the temperature ranges of 47–119 °C and 127–283 °C correspond to the loss of one crystal water molecule, and one coordinated water and two chloride molecule respectively.

The thermograms of (**C4**) and (**C5**) showed the first decomposition that may be accredited to the elimination of two coordinated water molecules with a mass loss up to 10.37 % (calcd. 10.71 %) in the temperature range 145–220 °C for **C5** and a mass loss of about 7.22 % (calcd. 7.68 %) in the temperature range 125–186 °C for **C4**. As for the thermogram of (**C5**), it showed a weight loss between 146 and 235 °C, agreeing with the presence of one water molecule in the coordination sphere + two chloride atoms (weight loss, 12.05 %, calcd. 13.02 %). The organic moiety of the complexes ($C_{17}H_{18}N_2O_3$) decomposes further with increasing temperature. The complete decomposition of the ligand occurs at above 400–700 °C, which suggests the formation of final decomposition products corresponding to the metal oxides [11,13,14,16,17]. The thermal outcomes are in good agreement with the theoretical formulae as projected from the analytical data. The reports of TGA information for the complexes (**C1–C5**) are summarized in Table 1.

3.8. DFT calculations

3.8.1. Optimized geometry

The optimized structures of the ligand and the related metal complexes are shown in Fig. 7. The changes in some of the selected bond lengths and angles are monitored from the ligand to the complexes. Among them is the change in the ligand C—O bonds that coordinate with the metal atoms, which changes in the order of **C4** (1.348 Å) > **C5** (1.346 Å) > **C1** = **HL** (1.345 Å) > **C2** (1.343 Å) > **C3** (1.336 Å). The change in the N—C bonds did not follow any specific order, thus the four N—C bonds in the ligand and complexes are characterized by different lengths and changes across the complexes. The metal-ligand bonds could be ranked in the following order **C5** (Ti) > **C2** (Ru) > **C3** (Fe) > **C1** (Cr) > **C4** (Al). Among the three enclosed bonds in the metal-ligand complexes, at least two follow the order of **C2** > **C3** > **C1, C5, C4** [46,47].

3.8.2. Frontier molecular orbitals

The frontier orbitals (HOMO and LUMO) exhibit a significant part in

the stability and reactivity of the molecules. The electron-withdrawing ability is categorized by LUMO, while the electron-donating ability is characterized by HOMO [46,48,49]. The feature of the HOMO and LUMO of the studied molecules are shown in Fig. 8. The HOMO and LUMO of the Schiff base ligand (**HL**) are located on the phenolate ring. The lowest energy absorption of **HL** is attributable to an intraligand charge transfer transition. In all the metal complexes, the HOMO is located around the metal atom and the coordinating atoms, except the complex **C4**. The LUMO of **C2, C3**, and **C4** are predominantly located on the methoxyphenyl ring, while **C4** shows an opposite behavior, as the HOMO is located on the methoxyphenyl moiety and the LUMO is on the phenolate ring. Both the HOMO and LUMO of **C1** are around the metal atom and the coordinating atoms [46,50,51]. The change in HOMO and LUMO energy levels is shown in Fig. 9 for the compounds. The molecular orbital calculations revealed that the complexes were more stable than the free ligand. The HOMO values were computed as −4.80, −5.66, −5.02, −5.74, and −3.65 eV for **C5** (Ti), **C2** (Ru), **C3** (Fe), **C1** (Cr), and **C4** (Al), respectively, whereas the LUMO values were 2.05, −1.98, −1.87, −3.15 and −2.02 eV Moreover, the values of ΔE for **C5, C2, C3, C1**, and **C4** were found to be 2.75, 3.68, 3.15, 2.59, and 1.64 eV correspondingly.

The smallest HOMO–LUMO gap was found for the complex **C4**, expected to exhibit greater catalytic activity as compared to the other complexes investigated. The lowest energy for the complex **C4** could be attributed to the metal-to-ligand charge transfer (MLCT) transition. It is observed that a decrease in the energy band gap brings about an increase in electrical conductivity. The HOMO of the metal complexes appears at a higher energy level and the LUMO at a lower energy level compared to the ligand, leading to lower energy band gap values of the metal complexes. The complex **C4** showed the highest HOMO energy and coupled with its relatively low LUMO energy level, which leads to the lowest energy band gap and most conductive of **C4** compared to the rest of the metal complexes. The complex **C1** exhibited the lowest LUMO and also the lowest HOMO among the metal complexes. Therefore, the order of the energy band gap is **HL** > **C2** > **C3** > **C5** > **C1** > **C4**.

3.6. Antioxidant capacity

Different procedures have been utilized for the evaluation of antioxidant activity in biological systems and foods as an avenue to monitoring a multiplicity of pathological happenings such as coronary heart disease, cellular grievance, atherosclerosis, and the aging route; these damaging incidences are free radicals causative [4,9,45]. Two kinds of free radicals are used for *in vitro* antioxidant activity studies of the Schiff base ligand (**HL**) and its trivalent metal complexes (**C1-C5**) *viz* DPPH-2, 2-diphenyl-1-picrylhydrazyl and ABTS-2,2′-azino-bis(3-ethyl-benzothiazoline-6-sulfonic acid). Ascorbic acid (vitamin C), Rutin, and Gallic acid were engaged as standard agents.

3.6.1. 2,2-diphenyl-1-picrylhydrazyl radical scavenging assay

Reactive oxygen species (ROS) have been well documented to be associated with the enteropathogenesis of various prolonged diseases like hypertension, coronary heart disease, and atherosclerosis [1,9,25]. The DPPH rummaging activity of the complexes was meaningfully advanced than that of the free ligand (**HL**), suggesting that the metal complexes (**C1-C5**) possess enhanced DPPH radical scavenging potential (Table 2). The scavenging potentials of **C1-C5**, and the standards amplified in a dose-dependent fashion (Fig. 4). The scavenging potential order could be ranked as: [Gallic acid] > [Vitamin C] > [**C2**] > [**C4**] > [G] > [**C5**] > [**HL**] > [**C3**] with the IC$_{50}$ ± SEM values being respectively 0.84 ± 1.73 > 1.17 ± 1.14 > 1.69 ± 2.68 > 1.98 ± 1.36 > 2.02 ± 1.47 > 2.21 ± 1.75 > 4.11 ± 1.58 > 5.74 ± 1.30 μM. The DPPH radical scavenging potentials of the as-synthesized compounds in this study showed results comparable to DPPH radical scavenging potentials of the Pt(IV), Ni(II), and Pd(II) complexes of Schiff base ligand (4-{2-[(2-hydroxy-benzylidene)-amino]-ethyl}-benzene-1,2-diol) as described by Kareem and co-workers [26]. The anti-radical studies
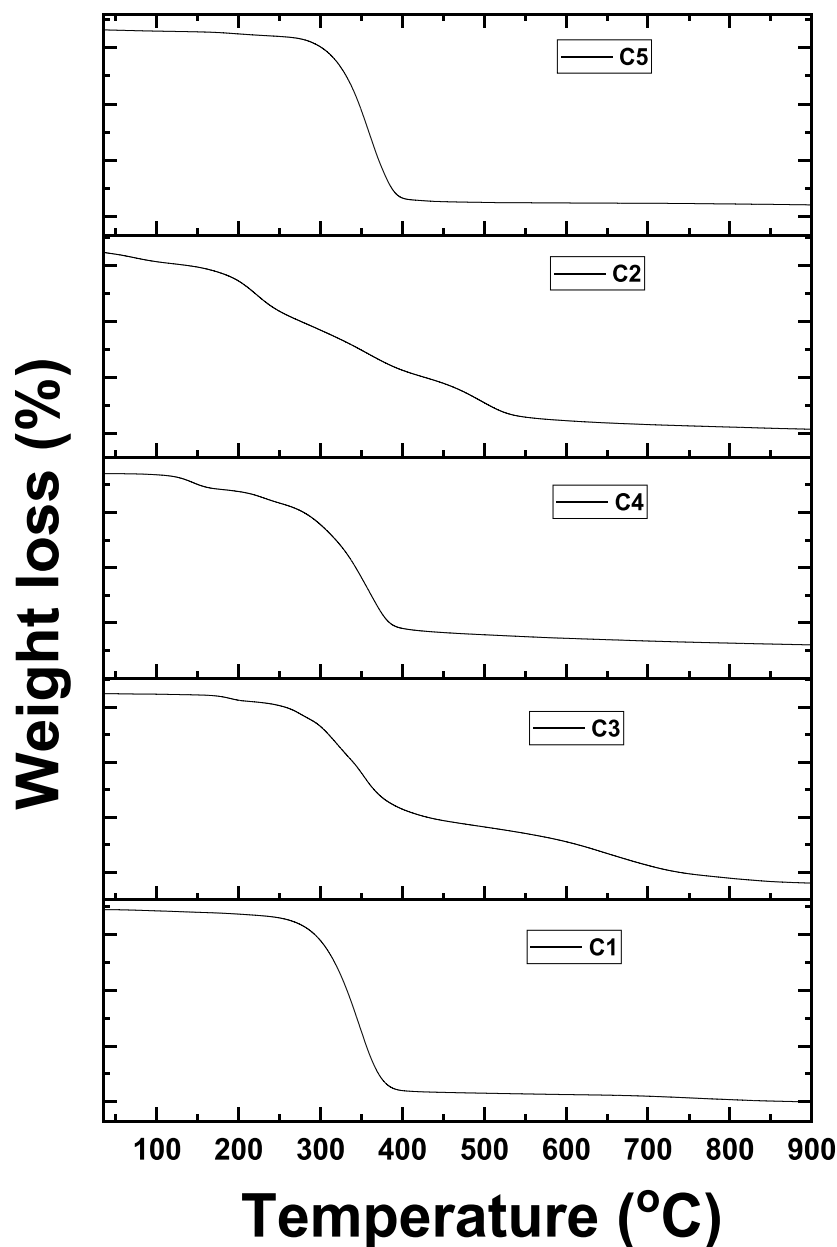
Fig. 3. TG curves of trivalent metal complexes (C1-C5) of HL Schiff base ligand.

revealed that the synthesized compounds might be considered promising agents for developing a therapeutic mediator for preventing cell oxidative impairment [4,15–17,23–25].

3.6.2. ABTS: 2,2′-Azino-bis(3-ethylbenzothiazoline-6-sulfonic acid) scavenging assay

The anti-radical potential of the synthesized compounds **HL** and (**C1–C5**) was further investigated as a means to enhance their radical scavenging potentials. The ABTS assay assesses the radical scavenging potentials by electron donation. The consequences of **HL** and M(III) activities on ABTS$^+$ radical are presented in Table 2 and displayed in Fig. 5. The bond interactions between the metal ions and the ligand (**HL**) brought about an increase in spectrum activity as compared to that of the free ligand (15.32 ± 5.3 μM) and a decrease in spectrum activity as compared to that of the standards used [Gallic acid (1.22 ± 1.08 μM), rutin (2.86 ± 0.92 μM)]. The uptake of the ABTS$^+$ radical by **HL** and **C1**-**C5** was established to possess modest to high activities [4,15]. However, **C5** presented significantly better ABTS scavenging activity with an IC$_{50}$

value of 8.70 ± 2.78 μM and a correlation coefficient of 0.976 R^2, while the remaining complexes **C2, C1, C3**, and **C4** gave IC$_{50} \pm$ SEM values of 8.81 ± 3.43, 10.49 ± 3.24, 12.02 ± 4.60 and 15.01 ± 4.98 μM, respectively. The ABTS rummaging activity arrangement can be hierarchical in the order of: [Gallic acid] > [Rutin] > [**C5**] > [**C2**] > [**C1**] > [**C3**] > [**C4**] > [**HL**]. The anti-radical investigation revealed that the synthesized compounds could play a chief role in therapeutic mediator development for pathological damage repair and aversion of cell oxidative damage [4,15]. Therefore, the results indicate that the complexes (**C2**) and (**C5**) exhibited enhanced antioxidant potential in comparison to **C1, C3, C4**, and the ligand (**HL**).

3.7. Antimicrobial analysis

The ligand (**HL**) and its corresponding trivalent complexes (**C1–C5**) were evaluated against bacterial and fungal species for their antibacterial and antifungal potentials, *via* the disk-diffusion agar method [33,34, 52,53], and ciprofloxacin was used as a standard drug. Strains

Table 1
Thermo-analytical results of the synthesized trivalent metal complexes.

Compound	Temperature range (°C)	DTA peak (°C)	Assignments
(C1)	220–422	343	Decomposition of ligand and formation of Cr_2O_3
(C2)	47–119	76	Loss of H_2O (crystal)
	127–283	221	Loss of H_2O (coordinated) + 2 chlorides
	295–428	360	Decomposition of ligand parts
	441–603	496	Decomposition of the remaining ligand with the formation of Ru_2O_3
(C3)	145–220	187	Loss of two H_2O molecules (coordinated)
	222–477	351	Loss of 1 chloride and diamine part of the ligand
	532–768	650	Decomposition of the remaining ligand with the formation of Fe_2O_3
(C4)	125–186	144	Loss of H_2O (coordinated)
	188–258	225	Loss of chloride and aldehyde part of ligand
	270–435	355	Decomposition of the remaining ligand with the formation of Al_2O_3
(C5)	146–235	184	Loss of H_2O (coordinated) + 2 chlorides
	260–425	360	Decomposition of the ligand with the formation of TiO_2

H_2O = water; C1 – C5 = Complexes.

Table 2
Antioxidant assessment of the free Schiff base (**HL**) and its trivalent metal complexes against DPPH and ABTS radicals.

Compound	DPPH scavenging activity		ABTS scavenging activity	
	$IC_{50} \pm SEM*$ (μM)	R^2	$IC_{50} \pm SEM*$ (μM)	R^2
(HL)	4.11 ± 1.58	0.925	15.32 ± 5.34	0.972
(C1)	2.02 ± 1.47	0.916	10.49 ± 3.24	0.939
(C2)	1.69 ± 2.68	0.971	8.81 ± 3.43	0.805
(C3)	5.74 ± 1.30	0.894	12.02 ± 4.60	0.977
(C4)	1.98 ± 1.36	0.889	15.01 ± 4.98	0.864
(C5)	2.21 ± 1.75	0.946	8.70 ± 2.78	0.976
Vitamin C**	1.17 ± 1.14	0.908	–	–
Rutin**	–	–	2.86 ± 0.92	0.962
Gallic acid**	0.84 ± 1.73	0.985	1.22 ± 1.08	0.948

* SEM = standard error mean (experiment run in triplícate); DPPH: 1,1-Diphenyl-2-picrylhydrazyl; ABTS: 2,2′-azinobis-3-ethylbenzothiazoline-6-sulfonic acid; IC_{50}: Inhibitory concentration at 50 %; R^2: correlation coefficient.
** = standard antioxidants; μM: micromolar.

investigated include the bacterial pathogens *E. coli, α-H. streptococcus*, and *S. aureus*, as well as the fungal pathogens *A. candideus, A. niger,* and *P. cephalosporin*. The antimicrobial potentials were considered in terms of inhibition zone values (mm) as described in Table 3 and depicted by a bar graph in Fig. 6. From the data, it can be perceived that the trivalent metal complexes affect a higher zone of inhibition (mm) than the free Schiff base (**HL**). However, the actions of the complexes (**C1-C5**) were found to be lower than that of the standard drug ciprofloxacin, against the bacteria strains evaluated in this study. It is worth noting that the pathogenic isolates were more sensitive (larger zone of inhibition) to [**C2**] than other complexes. The inhibition zones observed for **C2** were *E. coli* (20 mm)*, α-H. streptococcus* (10 mm)*, S. aureus* (16 mm)*, A. candideus* (8 mm)*, P. cephalosporin* (10 mm), and *A. niger* (8 mm). The highest antibacterial activity of the studied agents was observed against *S. aureus* and *E. coli*.

Furthermore, (**C2**) displayed the highest antifungal activity against *P. cephalosporin*, with an inhibition zone of 10 mm), whereas complexes (**C3**) and (**C4**) showed moderate antifungal actions (6 mm). The other complexes were found to be inactive against the fungal pathogens. In addition, (**C2**) was observed as the only compound to exhibit moderate

antifungal activities against fungal pathogens: *A. niger* and *A. candideus* with an inhibition zone of 8 mm. The observed results in the current study are in agreement with past reports presenting that higher antimicrobial activities were observed in standard drugs than in as-synthesized compounds [9–12,54]. In a study by Khanagwal et al. [17], it was conveyed that the europium(III) complexes performed as better agents than the ligand (L) and reference drugs investigated [17]. Zayed et al. [30] reported the *in vitro* antibacterial studies of [4, 4′-(((((ethane-1,2-diylbis(oxy))bis(2,1-phenylene))bis(methanylylidene))bis(azanylylidene))diphenol]ethane and its Cu(II), Mn(II), Zn(II), Ni(II), Co(II), Fe(III), and Cd(II) complexes against Gram-positive (*S. pyogones* and *B. subtilis*) and Gram-negative (*P. vulgaris* and *E. coli*) [30]. Inner metal- La(III), Yb(III), and Er(III) complexes of tetradentate (ONNO) Schiff base: 2,2′-((1*E*,1′*E*)-(1,3-phenylenebis(azanylylidene))bis (methanylylidene))diphenol have been reported to possess better antimicrobial activities against different organisms compared to the free ligand [27]. From the current study, it is seen that the antibacterial prospective of the complexes can be in the order of: [**C2**] > [**C5**] > [**C1**] > [**C3**] > [**C4**] > **HL**.

It is noteworthy to underscore that the expected enhanced lipophilic character of the large complexes could be answerable for their effective antimicrobial activity than the free ligand. Also, the vastly conjugated structure of auxiliary ligand (**HL**) with nitrogen and oxygen donor molecules increased the delocalization of π-electrons over the entire Schiff base ligand system, thus, it upsurges the lipid enticing tendency of the Ru(III), Cr(III), Fe(III), Ti(III), and Al(III) ions. The improved activity of the metal complexes as related to the free ligands can also be explicated on the distinctive Tweedy's chelation and Overtone's cell penetrability theories. Following this, M^{3+} ions penetrate the cell wall of microorganisms to the deep areas of the cell and thus deactivate diverse cellular enzymes which subsequently obstruct the growth of microbes. Coordination aids the polarisation of the metal ions decrease owing to the *partial* distribution of the positive charge (+ve) with the benefactor groups which in turn inhibit protein synthesis, and reduce the nutrient flow between the peripheral and interior partitions of the cells. This aids in improving the antimicrobial perspective of the metal complexes (**C1-C5**) as related to the ligand (**HL**) [5,6,11,14,15,17,45].

Ruthenium(III) complex (**C2**) showed higher antimicrobial properties against *S. aureus* and *E. coli* as compared to the other studied complexes. Additionally, it is the only compound to exhibit moderate antifungal activities against the fungal pathogens: *A. niger* and *A. candideus* with an inhibition zone of 8 mm as presented in Table 3. The higher antimicrobial potentials of **C2** could be correlated to the lipophilic nature increase resulting from the complexation of the ligand. Also, the activities of **C2** could be elucidated about the redox cycling reactions between Ru(III) and Ru(II) oxidation states, resulting in the establishment of reactive radical species leading to cell death [1,11,25,33,34,52–54].

3.9. Molecular docking

The most favorable binding conformation of the ligands (**HL, C2**, and **C5**) to the tested targets (**2XCT, 5BOD**, and **5L3J**) was considered in each case. The associated data of the decomposed energies as well as the binding affinities are enumerated in Table 4. The approximate free binding energy used in AutoDock4 is measured as a scoring function of the resulting linear combination: $\Delta G = \Delta G_{vdW} + \Delta G_{conform} + \Delta G_{Hbond} + \Delta G_{desolv} + \Delta G_{elec} + \Delta G_{tor}$, in which the molecular mechanics terms ΔG_{vdW}, $\Delta G_{conform}$, ΔG_{elec}, and ΔG_{Hbond} are the dispersion/repulsion, deviations from the covalent geometry electrostatic energies, and the hydrogen bonding, respectively. In addition, ΔG_{tor} represents the restriction of global rotation, internal rotors, and translation. Whereas, the ΔG_{desolv} term signposts the hydrophobic effect and desolvation. All the free binding energies were found to be negative, in the range of −4.96 to −6.10 kcal/mol for **2XCT**, with **C2** showing the highest value. Moreover, the binding energies of the studied compounds in the active sites of the
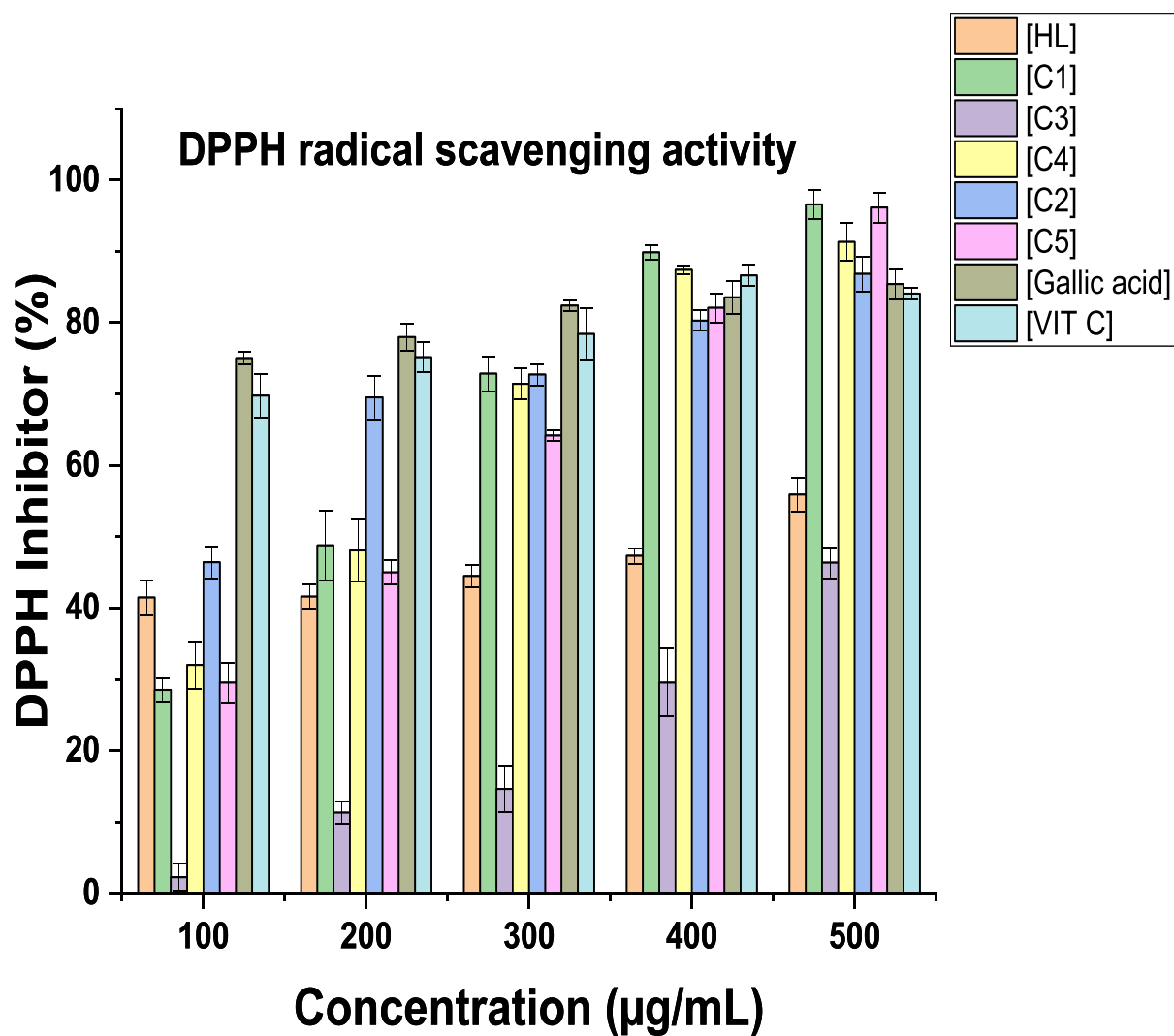
Fig. 4. DPPH free radical scavenging assays of HL and its M(III) complexes ($n = 3$).
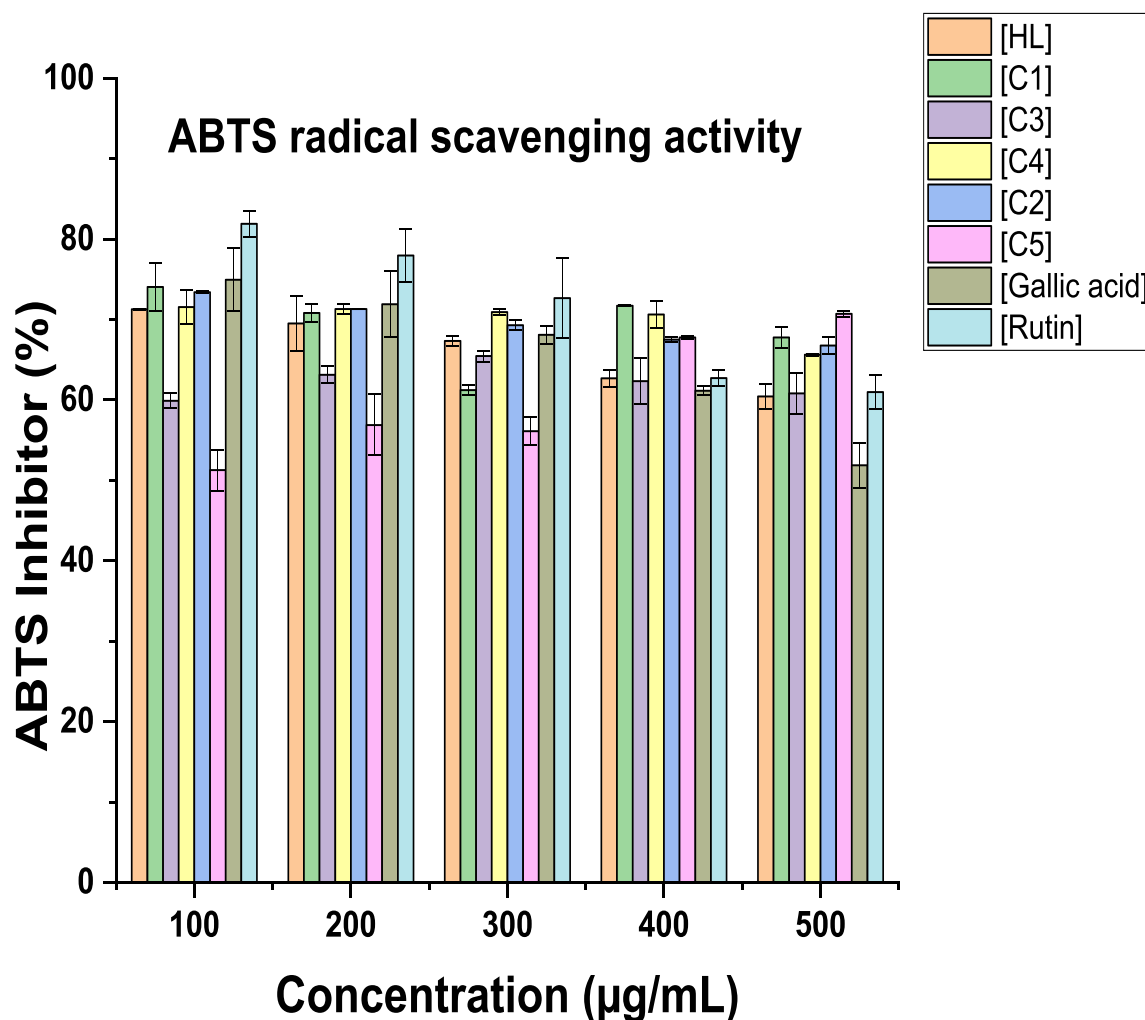
Fig. 5. ABTS activities of HL, trivalent metal complexes, and standard drugs ($n = 3$).

Table 3
Antimicrobial evaluation of the Schiff base (**HL**) and its trivalent metal complexes (**C1-C5**) against pathogenic microorganisms.

Compound	Inhibition zone (mm)					
	Bacteria			Fungi		
	S. aureus	*α-H. streptococcus*	*E. coli*	*A. niger*	*A. candideus*	*P. cephalosporin*
(**HL**)	8	5	7	–	–	–
(**C1**)	11	9	9	–	–	–
(**C2**)	16	10	20	8	8	10
(**C3**)	12	6	9	–	–	6
(**C4**)	8	7	7	–	–	6
(**C5**)	13	14	14	–	–	–
*Ciprofloxacin	22	25	20	-	-	-
*Fluconazole	-	-	-	16	20	24

* = **Standard drug**.

receptors **5BOD** and **5L3J** were found to vary from -5.68 to -7.24 kcal/mol for **5BOD** and from -5.73 to -6.26 kcal/mol for **5L3J**, with **HL** displaying slightly better docking scores than the other studied molecules for both cases [36–41]. The molecular docking results obtained from this study showed some similarity to other studies reporting Schiff bases and their metal complexes [2,26–30].

The docking results analyzed using Chimera software (Fig. 10) showed that **HL** interacts with **2XCT** through four N—H...O hydrogen bonds, varying from 1.908 Å to 2.767 Å and linking it to Met_{1121D} and

Arg_{1122D}, in which the studied molecule acted as hydrogen bonds' acceptor (Table S1). Moreover, being an H-bonds' donor, **HL** has built up an O—H...O interaction of 1.891 Å with the aminoacid residue Asp_{1083B} in the receptor **2XCT**. As for molecule **C2**, it binds to the binding pocket of **2XCT** via two N—H...O hydrogen bonds resulting from the residues Met_{1121B} and Arg_{1122B}, with the H...A distances being respectively equal to 1.933 Å to 2.125 Å Similarly, **C5** displayed two N—H...O hydrogen-bonding interactions with the same aminoacids (1.992 Å to 2.212 Å). In addition, the three molecules form hydrophobic interactions with the
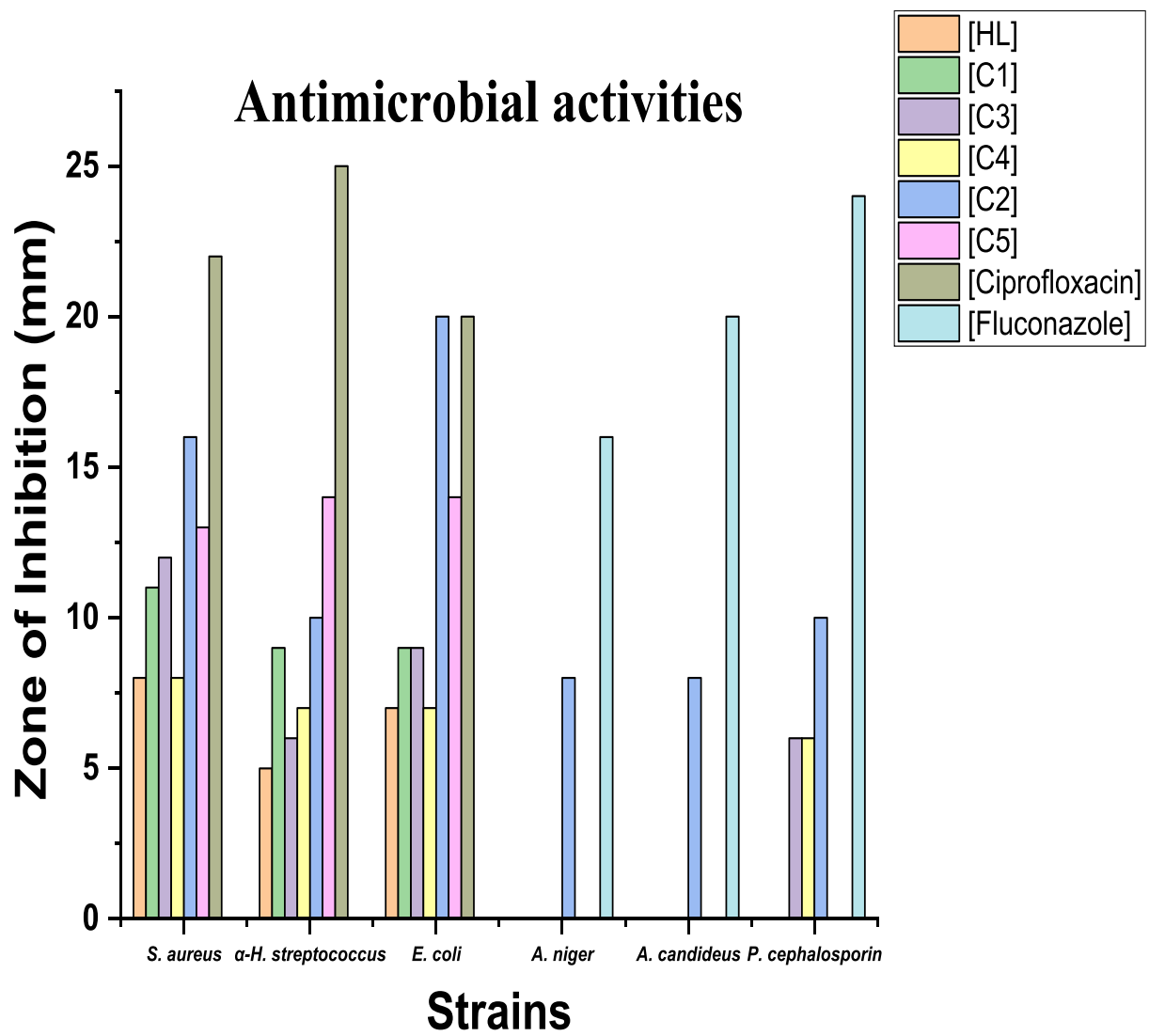
Fig. 6. Antimicrobial activity of the Schiff base (HL) and its M(III) complexes.
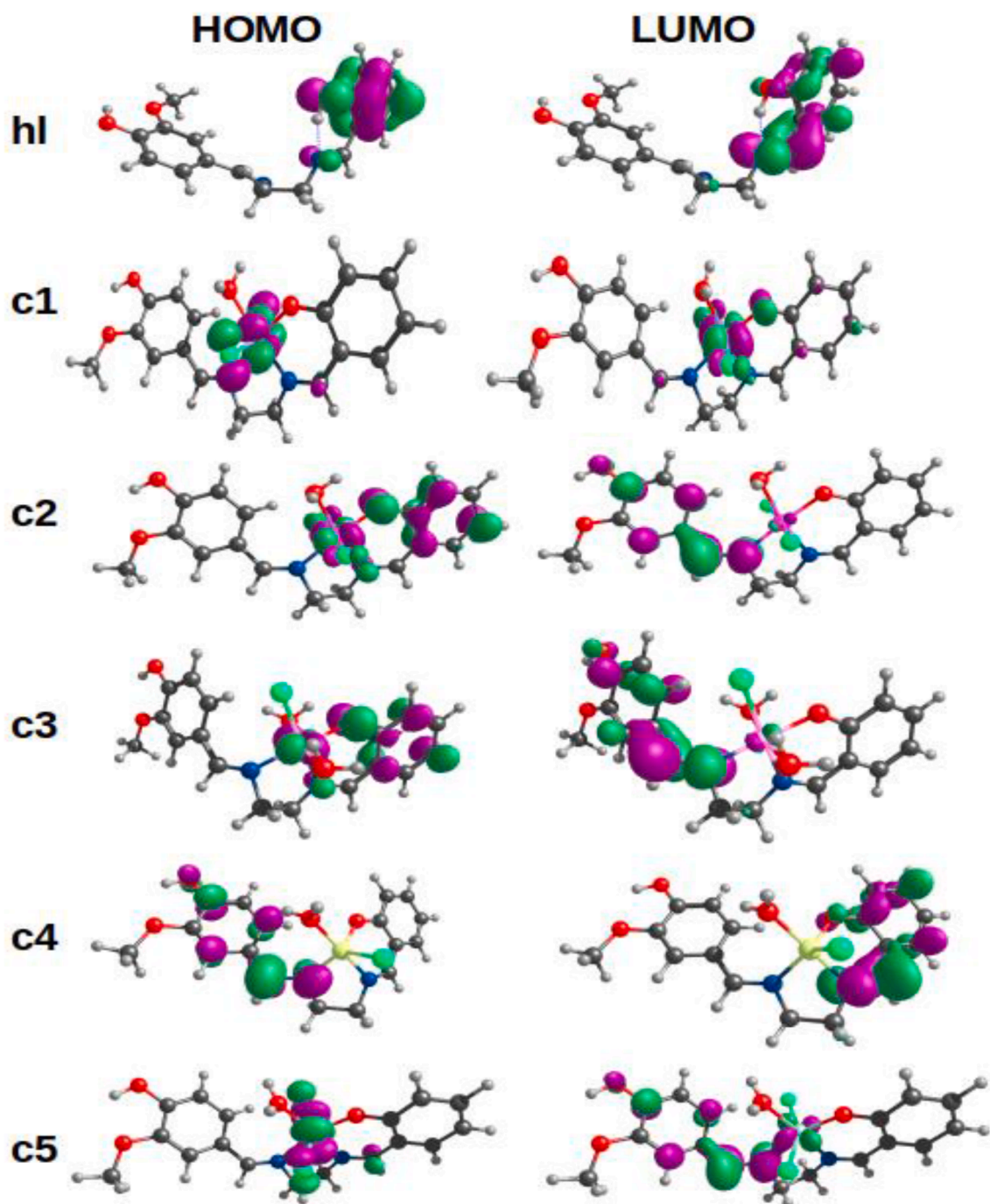
Fig. 7. Optimized structures of the ligand (HL) and metal complexes (C1-C5), showing the selected bond distances and angles.

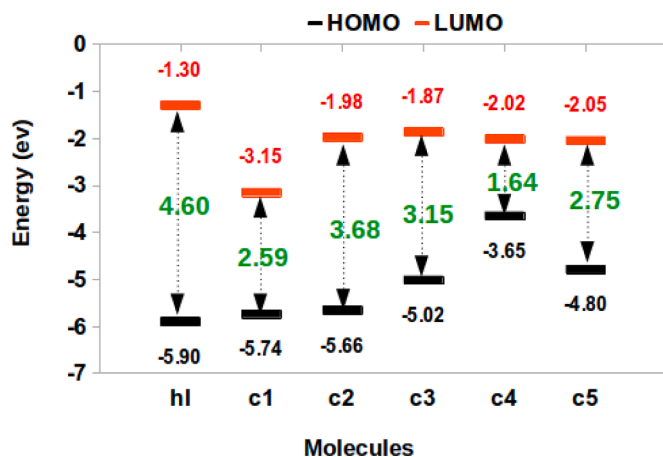**Fig. 8.** Electronic surface of the HOMO and LUMO for the ligand (HL) and metal complexes (C1-C5).

Fig. 9. The HOMO (black), LUMO (red), and the band gap (green) for the ligand HL and the metal complexes (C1-C5).

acceptor (Fig. 11). In addition, with **HL** being an H-bonds' donor, it interacts through three extra O—H...O interactions with Asp_{78A} and Ser_{124A}. We have observed that the residue Arg_{81A} acts as an H-bonds' donor and binds to **C2** and **C5** *via* three and two N—H...O hydrogen bonds respectively, varying from 2.206 Å to 3.237 Å in **C2** and from 2.055 Å to 3.111 Å for **C5**. Moreover, Asn_{51A} builds an O—H...O hydrogen-bonding interaction with **C2** (2.407 Å) and **C5** (2.228 Å), which acted as donors. An extra O—H...O H-bond was observed in both cases, between **C2** and Asp_{78A} as well as between **C5** and Glu_{55A}. Furthermore, the three molecules formed hydrophobic contacts observed mainly with the shared residues: Ile_{48A}, Asn_{51A}, Glu_{55A}, Asp_{78A}, Arg_{81A}, Val_{174A}, and Met_{183A} (Fig. S4).

In the case of the complexes resulting from the target **5L3J** and the ligands **HL, C2,** and **C5** (Fig. 12), we have noticed that the **5L3J-HL** complex pocket is held up through three O—H...O hydrogen-bonding connections comprising the H-bond acceptors' residues Asn_{46A} and Asp_{73A}, of 1.825 Å, 1.900 Å and 3.535 Å. Similarly, the complex **5L3J-C2** showed the presence of three O—H...O hydrogen bonds engaging both the aminoacid residues Val_{43A} and Asn_{46A} (2.263 Å, 2.161 Å and 3.004 Å). As for the complex **5L3J-C5**, the aminoacid Asn_{46A} acted as a

Table 4
Lowest binding affinities (kcal/mol) and the related decomposed component terms of the target-ligand complexes.

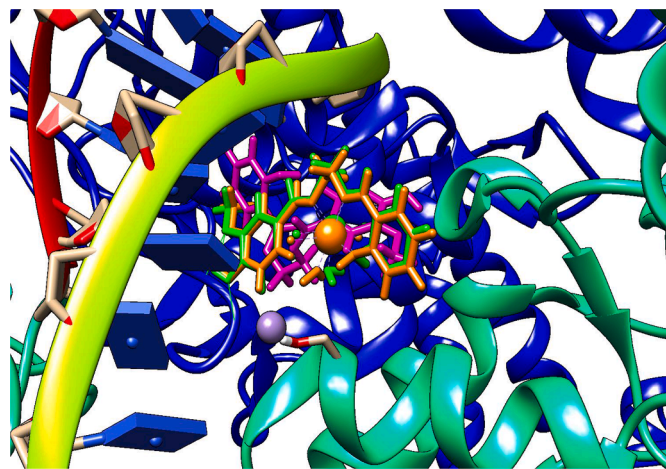|	ΔG	$\Delta G_{vdW} + \Delta G_{Hbond} + \Delta G_{desolv}$	ΔG_{elec}	$\Delta G_{intermol}$	$\Delta G_{tot\ int}$	ΔG_{tor}	$\Delta G_{unbound}$
Ligand/Receptor	**2XCT**						
HL	−4.96	−6.77	−0.58	−7.35	−1.58	+2.39	−1.58
C2	−6.10	−7.07	−0.13	−7.20	−1.70	+1.10	−1.70
C5	−6.00	−6.93	−0.16	−7.10	−0.92	+1.10	−0.92
	5BOD						
HL	−7.24	−9.35	−0.28	−9.63	−1.79	+2.39	−1.79
C2	−5.96	−7.53	−0.07	−7.61	−1.51	+1.65	−1.51
C5	−5.68	−7.53	−0.07	−7.60	−1.16	+1.92	−1.16
	5L3J						
HL	−6.26	−8.38	−0.27	−8.65	−1.98	+2.39	−1.98
C2	−6.18	−7.74	−0.08	−7.82	−1.63	+1.65	−1.63
C5	−5.73	−7.61	−0.04	−7.65	−1.27	+1.92	−1.27

Fig. 10. Overlapping of the three studied molecules in the receptor's binding pockets (HL is highlighted in magenta, C2 in green, and C5 in orange).

shared **2XCT**'s aminoacid residues: Asp_{1083B}, Asp_{1083D}, Tyr_{1087B}, Tyr_{1087D}, Glu_{1088B}, Ala_{1120D}, Met_{1121B}, Met_{1121D} and Arg_{1122D}, Asp_{73A}, Gly_{77A}, Ile_{78A}, Met_{91A}, Val_{120A}, Met_{166A}, Val_{167A} (Fig. S3).

As for the target **5BOD**, we have noticed that the ligand **HL** displayed two N—H...O H-bonds with the aminoacids Asn_{51A} and Gly_{82A} (2.111 Å and 1.981 Å), as well as one O—H...N hydrogen bond formed with the residue Ser_{124A} (3.208 Å), in which the studied molecule acted as an

H-bonds donor and acceptor as well, by forming respectively one N—H...O (2.651 Å) and two O—H...O (1.809 Å and 2.178 Å) hydrogen bonds with the studied molecule. An extra N—H...O interaction of 2.144 Å was observed with the residue Val_{120A} behaving as an H-bond donor (Fig. S5). In addition, the studied compounds interact with **5L3J**'s binding residues through hydrophobic contacts identified between the ligands and the following shared aminoacids: Asn_{46A}, Glu_{50A}, Asp_{73A}, Ile_{78A}, Pro_{79A}, Ile_{94A} and Val_{120A} (Fig. S5).

4. Conclusions

Cr(III), Ru(III), Fe(III), Al(III), and Ti(III)complexes (referred to as **C1-C5**) of the asymmetrical Schiff base ligand (**HL**), obtained from 2-hydroxybenzaldehyde and *o*-vanillin, were synthesized and characterized *via* different characterization techniques, namely elemental analysis, molar conductance, FT-IR spectroscopy, TG-DTG, and UV–Vis spectroscopy. The FTIR spectral data showed that the ligand **HL** coordinates to the trivalent metal ions *via* the azomethine group nitrogen atom and hydroxyl group oxygen atom of the *o*-vanillin moiety. The Schiff base acted as a tridentate ligand, and the resulting M(III) complexes exhibited an octahedral geometry. The complexes exhibited non-electrolytic characters in solution as depicted by the conductance measurements. The complete decomposition of the ligand occurs at above 400–700 °C, which suggests the formation of final products corresponding to the different metal oxides. The DFT calculations at B3LYP and LANL2DZ method for the ligand (**HL**) and metal complexes (**C1-C5**) support the experimental results of the geometric parameters. The lowest HOMO – LUMO energy band gap belongs to the complex **C4** and the most conductive complex is **C4** when compared to the rest of the metal complexes.
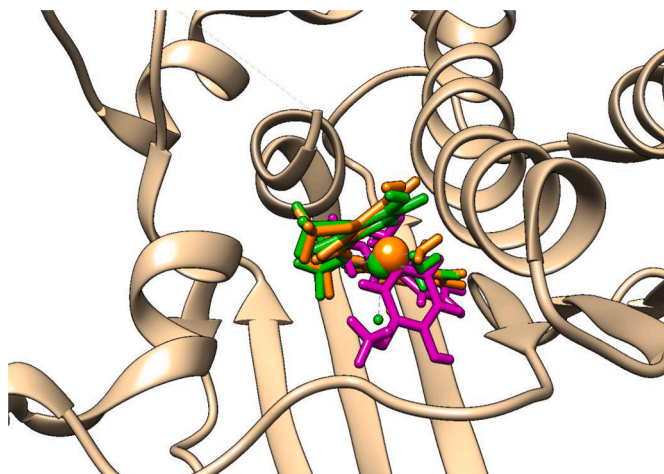
Fig. 11. Docking poses' overlap of the complexes' binding pockets built up of the studied molecules (HL, C2, C5) and the target 5BOD (HL is highlighted in magenta, C2 in green, and C5 in orange).
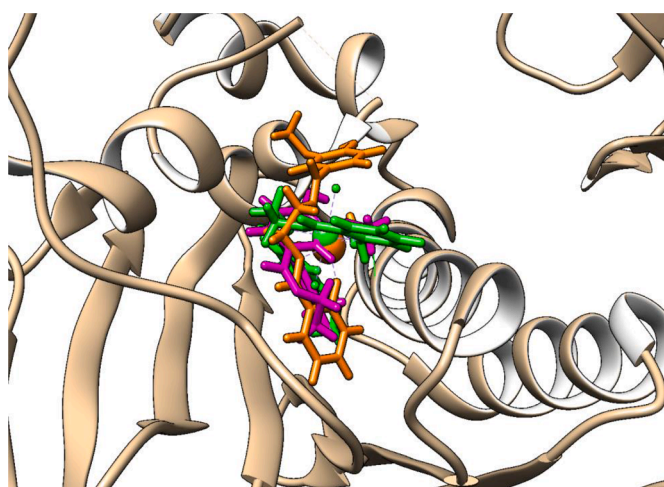
Fig. 12. Docking pose showing the overlapping of the three studied molecules HL, C2, and C5 in the binding pocket of 5L3J (HL is highlighted in magenta, C2 in green, and C5 in orange).

The antioxidant activity against DPPH and ABTS radicals established that the compounds possess a promising potential at averting radical formation. The synthesized metal(III) complexes demonstrated good to moderate antibacterial and antifungal activities against multidrug-resistant pathogens, particularly *E. coli, α-H. streptococcus, S. aureus, A. candideus, P. cephalosporin,* and *A. niger*. The better bactericidal and fungicidal potentials might be attributed to chelation potentials, considerably affecting the general biological behavior of the as-synthesized complexes. The complexes displayed good to excellent antioxidant and antimicrobial behaviors. Specifically, the antibacterial activities of **C2** and **C5** are a door opener to future investigation of the potential antibacterial and chemotherapeutic activities of these complexes. Moreover, to emphasize the interactions' categories that might bind the two most effective complexes **C2** and **C5** as well as their free ligand **HL** to the screened bacterial strains, a molecular docking simulation was carried out against selected pathogenic proteins from each species investigated, namely *Staphylococcus aureus* topoisomerase II DNA gyrase A (PDB ID: 2XCT), *Streptococcus pneumoniae* topoisomerase II DNA gyrase B (PDB ID: 5BOD) and E. *coli* topoisomerase II DNA gyrase B (PDB ID: 5L3J). the docking results showed good binding energies and promising maximum interactions, particularly classical N—H...O and

O—H...O hydrogen bonds, alongside the hydrophobic contacts.

CRediT authorship contribution statement

Ikechukwu P. Ejidike: Writing – review & editing, Writing – original draft, Visualization, Validation, Software, Methodology, Investigation, Formal analysis, Conceptualization. **Amani Direm:** Writing – review & editing, Visualization, Validation, Software, Methodology, Formal analysis. **Cemal Parlak:** Writing – review & editing, Visualization, Validation, Software, Methodology, Formal analysis. **Adebayo A. Adeniyi:** Writing – review & editing, Visualization, Validation, Software, Methodology, Formal analysis. **Mohammad Azam:** Writing – review & editing, Visualization, Validation, Resources. **Athar Ata:** Writing – review & editing, Visualization, Validation, Supervision, Resources, Funding acquisition. **Michael O. Eze:** Writing – review & editing, Visualization, Validation, Supervision, Resources. **Joshua W. Hollett:** Resources, Supervision, Validation, Visualization, Writing – review & editing. **Hadley S. Clayton:** Writing – review & editing, Visualization, Validation, Supervision, Resources, Funding acquisition.

Declaration of competing interest

The authors declare that they have no identified competing personal relationships or financial interests that could have appeared to impact the work reported in this paper.

Data availability

Data will be made available on request.

Supplementary materials

Supplementary material associated with this article can be found, in the online version, at doi:10.1016/j.chphi.2024.100549.

References

[1] I.P. Ejidike, P.A. Ajibade, Synthesis, characterization, *in vitro* antioxidant and anticancer studies of ruthenium(III) complexes of symmetric and asymmetric tetradentate Schiff bases, J. Coord. Chem. 68 (14) (2015) 2552–2564.

[2] B. Kumar, J. Devi, A. Manuja, Synthesis, structure elucidation, antioxidant, antimicrobial, anti-inflammatory and molecular docking studies of transition metal (II) complexes derived from heterocyclic Schiff base ligands, Res. Chem. Intermed. 49 (2023) 2455–2493.

[3] Eid H. Alosaimi, A.A. Alsibaai, M.S. El-Shahawi, M.S. Refat, Synthesis, physicochemical and thermal analyses of Ru(III), Pt(IV), and Ir(III) complexes with NO bidentate Schiff base ligand, Russ. J. Phys. Chem. A 92 (11) (2018) 2227–2236.

[4] I.P. Ejidike, P.A. Ajibade, Synthesis, spectroscopic, antibacterial and free radical scavenging studies of Cu(II), Ni(II), Zn(II) and Co(II) complexes of 4,4′-{ethane-1,2-diylbis[nitrilo(1*E*)eth-1-yl-1-ylidene]}dibenzene-1,3-diol Schiff base, J. Pharm. Sci. Res. 9 (2017) 593–600.

[5] S.R. Kelode, Synthesis, characterization and antimicrobial activity Cr(III), Mn(III), Fe(III), VO(IV), Zr(IV) and UO$_2$(VI) metal complexes derived from bidentate thiazole Schiff base, J. Chem. Pharm. Res. 5 (7) (2013) 100–103.

[6] P. Mittal, S. Joshi, V. Panwar, V. Uma, Biologically active Co(II), Ni(II), Cu(II) and Mn(II) complexes of Schiff bases derived from vinyl aniline and heterocyclic aldehydes, Int. J. ChemTech Res. 1 (2009) 225–232.

[7] M. Lashanizadegan, M. Jamshidbeigi, Template synthesis of unsymmetrical tetradentate Schiff base complexes of Ni(II), Co(II), Zn(II) and X-ray structure of Ni (II) complex, J. Sci. Islam. Repub. Iran 22 (2011) 121–124.

[8] N. Raman, A. Sakthivel, N. Pravin, Exploring DNA binding and nucleolytic activity of few 4-aminoantipyrine based amino acid Schiff base complexes: a comparative approach, Spectrochim. Acta A Mol. Biomol. Spectrosc. 125 (2014) 404–413.

[9] I.P. Ejidike, P.A. Ajibade, Synthesis and *in vitro* anticancer, antibacterial, and antioxidant studies of unsymmetrical Schiff base derivatives of 4-[(1*E*)-*N*-(2-aminoethyl)ethanimidoyl]benzene-1,3-diol, Res. Chem. Intermed. 42 (8) (2016) 6543–6555.

[10] Y. Pin, Z. Xiaoping, Synthesis and characterization of new Chrominum(III), Vanadium(W), and Titanium(III) complexes with biologically active isonicotinic acid hydrazide, J. Inorg. Biochem. 37 (1989) 61–68.

[11] E. Keskioglu, A.B. Gunduzalp, S. Cete, F. Hamurcu, B. Erk, Cr(III), Fe(III) and Co (III) complexes of tetradentate (ONNO) Schiff base ligands: synthesis, characterization, properties and biological activity, Spectrochim. Acta A Mol. Biomol. Spectrosc. 70 (2008) 634–640.

[12] L.A. Saghatforoush, A. Aminkhan, F. Chalabian, Iron(III) Schiff base complexes with asymmetric tetradentate ligands: synthesis, spectroscopy, and antimicrobial properties, Transit. Met. Chem. 34 (2009) 899–904.

[13] S. Santhi, C.G.R. Namboori, Synthesis, characterization and spectral studies of Fe (III) and Cr(III) Schiff base complexes with acetoacetanilidoethylenediamine, Orient. J. Chem. 27 (3) (2011) 1203–1208.

[14] Z. Asadi, M. Asadi, M.R. Shorkaei, Synthesis, characterization and DFT study of new water-soluble aluminum(III), gallium(III) and indium(III) Schiff base complexes: effect of metal on the binding propensity with bovine serum albumin in water, J. Iran. Chem. Soc. 13 (2016) 429–442.

[15] I.P. Ejidike, P.A. Ajibade, Synthesis, characterization, anticancer and antioxidant studies of Ru(III) complexes of monobasic tridentate Schiff bases, Bioinorg. Chem. Appl. 2016 (2016) 9672451. Article ID.

[16] I.V. Esther, P.N. Naomi, A.O. Aliu, A.S. Olufunke, Synthesis, characterization and antimicrobial studies of a Schiff base derived from 1,8-diaminonaphthalene and 2-hydroxy-1-naphthaldehyde with its metal complexes, Int. J. Chemtech Res. 12 (3) (2019) 72–79.

[17] J. Khanagwal, S.P. Khatkar, P. Dhankhar, M. Bala, R. Kumar, P. Boora, V.B. Taxak, Synthesis and photoluminescence analysis of europium(III) complexes with pyrazole acid and nitrogen containing auxiliary ligands, Spectrosc. Lett. 53 (2020) 625–647.

[18] A.W. Zoubi, Y.G. Ko, Self-assembly of hierarchical N-heterocycles-inorganic materials into three-dimensional structure for superior corrosion protection, Chem. Eng. J. 356 (2019) 850–856.

[19] A.W. Zoubi, M.E. Khan, Y.G. Ko, A simple method to functionalize the surface of plasma electrolysis produced inorganic coatings for growing different organic structure, Prog. Org. Coat. 171 (2022) 107008.

[20] A.W. Zoubi, M.P. Kamil, S. Fatimah, N. Nashrah, Y.G. Ko, Recent advances in hybrid organic-inorganic materials with spatial architecture for state-of-the-art applications, Prog. Mater. Sci. 112 (2020) 100663.

[21] A.W. Zoubi, A.W. Allaf, B. Assfour, Y.G. Ko, Toward two-dimensional hybrid organic-inorganic materials based on a I-PE/UHV-PVD system for exceptional corrosion protection, Appl. Mater. Today 24 (2021) 101142.

[22] S. Roy, S. Javed, M.M. Olmstead, A.K. Patra, First structural example of a metal uncoordinated mesoionic imidazo[1,5-a]pyridine and its precursor intermediate copper complex: an insight to the catalytic cycle, Dalton Trans. 40 (2011) 12866–12876.

[23] A.A. Al-Amiery, Synthesis and antioxidant, antimicrobial evaluation, DFT studies of novel metal complexes derivative from Schiff base, Res. Chem. Intermed. 38 (2012) 745–759.

[24] Y. Cetinkaya, H. Gocer, A. Menzek, I. Gulcin, Synthesis and antioxidant properties of (3,4-dihydroxyphenyl)(2,3,4-trihydroxyphenyl)methanone and its derivatives, Arch. Pharm. 345 (2012) 323–334.

[25] E. Akila, M. Usharani, R. Rajavel, Metal (II) complexes of bioinorganic and medicinal relevance: antibacterial, antioxidant and DNA cleavage studies of tetradentate complexes involving O, N-donor environment of 3,3′-dihydroxybenzidine-based Schiff bases, Int. J. Pharm. Sci. 5 (2013) 573–581.

[26] M.J. Kareem, A.A.S. Al-Hamdani, V.Y. Jirjees, M.E. Khan, A.W. Allaf, W.A Zoubi, Preparation, spectroscopic study of Schiff base derived from dopamine and metal Ni(II), Pd(II), and Pt(IV) complexes, and activity determination as antioxidants, J. Phys. Org. Chem. 34 (3) (2021) e4156.

[27] M.A. Diab, G.G. Mohamed, W.H. Mahmoud, A.Z. El-Sonbati, Sh.M. Morgan, S. Y. Abbas, Inner metal complexes of tetradentate Schiff base: synthesis, characterization, biological activity and molecular docking studies, Appl. Organomet. Chem. 33 (7) (2019) e4945.

[28] A. Fatima, G. Khanum, D.D. Agrawal, S.K. Srivastava, R.J. Butcher, S. Muthu, M. Ahmad, K. Althubeiti, N. Siddiqui, S. Javed, Synthesis, spectroscopic, crystal structure, DFT, hirshfeld surface and molecular docking analysis of hexahydroquinoline derivative (HQ), Polycycl. Aromat. Compd. 43 (5) (2023) 4242–4270.

[29] A. Fatima, G. Khanum, I. Verma, R.J. Butcher, N. Siddiqui, S.K. Srivastava, S. Javed, Synthesis, characterization, crystal structure, hirshfeld surface, electronic excitation, molecular docking, and DFT studies on 2-amino thiophene derivative, Polycycl. Aromat. Compd. 43 (2) (2023) 1644–1675.

[30] E.M. Zayed, A.M.M. Hindy, G.G. Mohamed, Molecular structure, molecular docking, thermal, spectroscopic and biological activity studies of bis-Schiff base ligand and its metal complexes, Appl. Organomet. Chem. 32 (1) (2018) e3952.

[31] Gaussian 09W, Gaussian Inc, Wallingford CT, USA, 2009.

[32] A. Frisch, A.B. Nielson, A.J. Holder, Gauss View User Manual, Gaussian Inc, Pittsburgh USA, 2000.

[33] I.P. Ejidike, H.S. Clayton, Green synthesis of silver nanoparticles mediated by *Daucus carota* L.: antiradical, antimicrobial potentials, *in vitro* cytotoxicity against brain glioblastoma cells, Green Chem. Lett. Rev. 15 (2) (2022) 297–310.

[34] A. Hossan, M. Alsahag, A. Alisaac, M.A. Bamaga, A.I. Alalawy, N.M. El-Metwaly, Synthesis, molecular modelling and biological evaluation of new4-aminothiophene and thienopyrimidine compounds, J. Taibah Univ. Sci. 17 (1) (2023) 2164993.

[35] G.M. Morris, R. Huey, W. Lindstrom, M.F. Sanner, R.K. Belew, D.S. Goodsell, A. J. Olson, Autodock4 and AutoDockTools4: automated docking with selective receptor flexiblity, J. Comput. Chem. 16 (2009) 2785–2791.

[36] B.D. Bax, P.F. Chan, D.S. Eggleston, A. Fosberry, D.R. Gentry, F. Gorrec, I. Giordano, M.M. Hann, A. Hennessy, M. Hibbs, J. Huang, E. Jones, J. Jones, K. K. Brown, C.J. Lewis, E.W. May, M.R. Saunders, O. Singh, C. Spitzfaden, C. Shen, A. Shillings, A.F. Theobald, A. Wohlkonig, N.D. Pearson, M.N. Gwynn, Type Iia Topoisomerase inhibition by a new class of antibacterial agents, Nature 466 (2010) 935.

[37] G.Y. Chen, F.M. Ng, Y.W. Tan, A. Poulsen, W. Seetoh, G. Lin, C. Kang, S.W. Then, N. H. Ahmad, Y.L. Wong, H.Q. Ng, B.C.S. Chia, Q.Y. Lau, J. Hill, A.W. Hung, T. H. Keller, Application of fragment-based drug discovery against DNA GyraseB, Chempluschem 80 (8) (2015) 1250–1254.

[38] M. Gjorgjieva, T. Tomasic, M. Barancokova, S. Katsamakas, J. Ilas, P. Tammela, L. Peterlin Masic, D. Kikelj, Discovery of benzothiazole scaffold-based DNA gyrase B inhibitors, J. Med. Chem. 59 (2016) 8941–8954.

[39] A. Kumar, U. Bora, Molecular docking studies of curcumin natural derivatives with DNA topoisomerase I and II-DNA complexes, Interdiscip. Sci. 6 (4) (2014) 285–291.

[40] C. Sissi, M. Palumbo, In front of and behind the replication fork: bacterial type IIa topoisomerases, Cell Mol. Life Sci. 67 (2010) 2001–2024.

[41] D. Klostermeier, Why Two? On the Role of (A-) symmetry in negative supercoiling of DNA by Gyrase, Int. J. Mol. Sci. 19 (2018) 1489.

[42] H.M. Berman, J. Westbrook, Z. Feng, G. Gilliland, T.N. Bhat, H. Weissig, I. N. Shindyalov, P.E. Bourne, Nucleic Acids Res. 28 (1) (2000) 235–242.

[43] T.D. Goddard, C.C. Huang, T.E. Ferrin, Visualizing density maps with UCSF chimera, J. Struct. Biol. 157 (2007) 281–287.

[44] A.C. Wallace, R.A. Laskowski, J.M. Thornton, LIGPLOT: a program to generate schematic diagrams of protein-ligand interactions, Protein Eng. 8 (1996) 127–134.

[45] X. Xia, L. Xia, G. Zhang, J. Xu, C. Wang, Y. Wu, K. Zhao, V. Uma, Preparation, structure and antioxidant property of manganese(II) and zinc(II) complexes with bis(N-ethylbenzimidazol-2-ylmethyl)allylamine, J. Coord. Chem. 73 (24) (2020) 3322–3331.

[46] S.S. Sabar, O.I. Alajrawy, S.A.H. Elbohy, C.M. Sharaby, New molybdenum(VI) and vanadium(IV) complexes with 3-aminopyridine and dithiooxamide ligands spectroscopic characterization, DFT calculations, and *in vitro* cytotoxic activity, Mater. Today Proc. 65 (2022) 2537–2550.

[47] V. Sundarpal, B. Shashi kanth, N. Rajitha, Yadagiri, B. spectroscopic characterization, DNA binding and DFT/PCM calculations of new hydrogen-bonded charge transfer complex between 4-dimethylaminopyridine and chloranilic acid, Results Chem. 5 (2023) 100694.

[48] S. Premkumar, T.N. Rekha, R.M. Asath, T. Mathavan, A.M.F. Benial, Vibrational spectroscopic, molecular docking and density functional theory studies on 2-acetylamino-5-bromo-6-methylpyridine, Eur. J. Pharm. Sci. 82 (2016) 115.

[49] M. Varukolu, M. Palnati, V. Nampally, S. Gangadhari, M. Vadluri, P. Tigulla, New charge transfer complex between 4-Dimethylaminopyridine and DDQ: synthesis, spectroscopic characterization, dna binding analysis, and density functional theory (DFT)/Time-Dependent DFT/Natural transition orbital studies, ACS Omega 7 (1) (2021) 810–822.

[50] J.R. Anacona, M. Loroño, D. Marpa, C. Ramos, F. Celis, Synthesis, characterization, density functional theory calculations, and *in vitro* antibacterial activity of novel transition metal complexes containing an O₃-tridentate amoxicillin-based Schiff base: a silver(II) complex as alternative against Pseudomonas aeruginosa resistant to amoxicillin, Appl. Organomet. Chem. (2020) e5755.

[51] B. Anandhan, T. Sumathi, P. Sivakumar, S. Kamatchi, Synthesis, molecular structure and multiple biological activities of β-cycloketols using methylamine catalyst, J. Mol. Struct. 1286 (2023) 135497.

[52] M. Alias, H. Kassum, C. Shakir, Synthesis, physical characterization and biological evaluation of Schiff base M(II) complexes, J. Assoc. Arab Univ. Basic Appl. Sci. 15 (2014) 28–34.

[53] Neelofar, N. Ali, S. Ahmad, N.M. AbdEl-Salam, R. Ullah, R. Nawaz, S. Ahmad, Synthesis and evaluation of antioxidant and antimicrobial activities of Schiff base tin (II) complexes, Trop. J. Pharm. Res. 15 (12) (2016) 2693–2700.

[54] I.P. Ejidike, M.O. Bamigboye, H.S. Clayton, Spectral, *in vitro* antiradical and antimicrobial assessment of copper complexes containing tridentate Schiff base derived from dihydroxybenzene functionality with diaminoethylene bridge, Spectrosc. Lett. 54 (3) (2021) 212–230.